SECOND ORDER PURE LAGRANGE-GALERKIN METHODS FOR FLUID-STRUCTURE INTERACTION PROBLEMS

MARTA BENÍTEZ† AND ALFREDO BERMÚDEZ‡

Abstract. In this paper we propose a second order (both in time and in space) pure Lagrange-Galerkin method for the numerical solution of fluid-structure interaction problems. The proposed scheme is written in material coordinates and in terms of displacements in the structure and of displacements and pressures in the fluid. Pure-Lagrangian displacement methods are useful for solving free surface problems and fluid-structure interaction problems because the computational domain is independent of time and fluid-structure coupling at the interphase is straightforward. Unfortunately, for moderate to high-Reynolds number flows, pure-Lagrangian methods can lead to high distortion of the mesh elements and as a consequence non-accurate approximations can be obtained. Before this happens it is necessary to re-mesh and re-initialize the motion. In the present paper we also deal with this problem by proposing a method to be combined with the pure Lagrange-Galerkin method we introduce that preserves the order. In order to assess the performance of the overall numerical method, we solve different problems in two space dimensions. In particular, numerical results for the two-dimensional motion of an elastic circular cylinder in a fluid and a sloshing problem with an elastic submerged cylinder in a rectangular tank are presented.

Key words. fluid-structure interaction problems, Navier-Stokes equations, linear elasticity, Lagrange-Galerkin methods, second-order schemes, pure-Lagrangian methods, semi-Lagrangian methods

AMS subject classifications. 65M25, 65M60, 74F10

1. Introduction. In the present paper a new pure Lagrange-Galerkin method to solve fluid-structure interaction problems is described. Important problems from different fields of engineering and applied sciences involve the interaction of fluids and structures. Examples are common in off-shore structures, liquid containers, airplanes, submarines, etc. Typically, the fluid model is based on a Eulerian formulation in terms of the velocity in contrast to the usual Lagrangian formulation in terms of the displacement for the solid model. Therefore, a typical difficulty for solving fluid-structure interaction problems is coupling at the interphase. Moreover, often the fluid problem is a free surface problems. The Eulerian formulation of these problems presents two classical difficulties: the treatment of the convective term and the modelling and tracking of the free surface. All these problems disappear if the fluid problem is written in Lagrangian coordinates and in terms of displacement.

The methods of characteristics are extensively used for solving convection-diffusion problems with dominant convection (see the review paper [12]). These methods are based on time discretization of the time derivative along characteristic curves. When they are referred to a fixed domain (respectively, to a time dependent domain) they are called pure Lagrangian methods (respectively, semi-Lagrangian methods). The classical methods of characteristics are formulated in Eulerian coordinates and therefore they are semi-Lagrangian schemes. These methods have been mathematically analyzed and applied to different problems with time independent domains by several authors (see [11], [23], [29], [27], [7], [8] and [3]). More precisely, in [29] and [23] the classical first order characteristic method, as introduced in [11], is combined with finite elements for solving convection-diffusion equations. In [27], [7] and [8] a second order characteristics method for solving constant coefficient convection-diffusion equations is analyzed. Stability and optimal error estimates are proved.

The Eulerian framework of the classical characteristics methods is unduly cumbersome to solve problems with time dependent domains, such as free-surface flows or problems involving interfaces between different bodies. These problems have been solved with several Lagrangian approaches. More precisely, in [15], [20], [26], [18], [19], [17], [10], [22] the Eulerian classical formulation of the Navier-Stokes equations is considered and the classical technique to discretize the material derivative is used. A Lagrangian framework is considered because the track of the locations of individual particles (which can be nodes) is kept and particles in current domain are viewed as moving points from previous domains. The particle positions are updated by using the values of velocity. At each time step, the problem to solve is non-linear because it is written in the current domain which is unknown (it depends on current velocity, unknown too). Notice that the particle finite element method (PFEM) uses this strategy to discretize the convective term. This method has been applied to the solution of fluid-dynamics problems including free surface flows and breaking waves [18], fluid-structure interactions ([19], [17]) or fluid-object interactions

†Departamento de Matemáticas, Universidade da Coruña, c/ Mendizábal s/n, 15403 Ferrol, Spain (marta.benitez@udc.es)

‡Departamento de Matemática Aplicada, Universidade de Santiago de Compostela, c/ Lope Gómez de Marzoa s/n, 15786 Santiago de Compostela, Spain (alfredo.bermudez@usc.es)

([10], [22]). On the other hand, in [25] the Lagrangian form of the Navier-Stokes equations in terms of the motion is considered. A Newmark's algorithm for time discretization, combined with element finite, is proposed to solve the Lagrangian problem. At each time step, the obtained problem is non-linear and it is solved by Newton-Raphson iteration. In this paper, we also consider the Lagrangian form of the Navier-Stokes equations but in terms of displacement. Moreover, we propose a new strategy of time discretization so that at each time the problem to solve is linear.

In the past, the main problem of pure Lagrangian methods for fluids has been the lack of re-meshing (see [15] and [26]). As an exception, in [20] a rezoning technique has been applied for the propagation analysis of solitary waves. Advances in meshing have enabled the automated and adaptive re-meshing, which extends the range of application of Lagrangian methods (see, for instance, [25] and [18]). More precisely, in [25] a full Lagrangian finite element method for the analysis of Newtonian flows based on continuous and adaptive re-meshing is developed. Numerical results for a sloshing problem and a for the propagation of a water wave are presented. The finite element mesh is maintained undistorted throughout the computation by recourse to frequent and adaptive re-meshing. On the other hand, in the particle finite element method (PFEM) the mesh is regenerated at every time-step, the particles belonging to the boundaries may change and the new boundary nodes (and therefore the particles) have to be identified (see [18] for details).

Recently, we have introduced new characteristics methods combined with finite elements to solve time dependent domain problems, first for scalar linear convection-diffusion equations and then for vector nonlinear convection-diffusion equations. All these methods are linear and are obtained by introducing a change of variable from the current configuration to a reference configuration (known). In particular, for scalar linear convection-diffusion equations, a second order pure Lagrange-Galerkin scheme has been introduced in [4] and [5] where stability and optimal error estimates were proved. In [9], semi-Lagrangian and pure-Lagrangian methods are also proposed and analyzed for convection-diffusion equations. In [4] and [5] more general problems are considered. Specifically, we have considered a (possibly degenerate) variable coefficient diffusive term instead of the simpler Laplacian, general mixed Dirichlet-Robin boundary conditions, and a time dependent domain. Moreover, we have analyzed a scheme with approximate characteristic curves and presented numerical results for pure-Lagrangian and semi-Lagrangian methods. In [6] a unified approach to state pure-Lagrangian and semi-Lagrangian methods for solving convection-diffusion partial differential equations is introduced. More precisely, a quite general change of variable from the current configuration to a reference configuration, not necessarily the one of the initial time, is proposed obtaining another new strong formulation of the problem from which classical and new time discretization methods can be introduced in a natural way. Moreover, stability estimates for the pure-Lagrangian method proposed in [4] and [5] have been obtained.

By applying the above ideas to the Navier-Stokes equations, we can obtain displacement methods similar to those used for numerical solution of solid mechanics problems. More precisely, in [2] a unified formulation to introduce Lagrangian and semi-Lagrangian velocity and displacement methods for solving the Navier-Stokes equations is proposed. By using this formulation, two new second-order characteristics methods in terms of the displacement and classical second-order characteristics methods in terms of the velocity are obtained. Moreover, numerical results showing the performance of these methods are presented.

In this paper, we consider the coupling of a viscous Newtonian incompressible fluid and a linear elastic solid. The governing equations for the fluid are the unsteady incompressible Navier-Stokes equations and, for the solid, the Navier-Lamé equations of linear elastodynamics. These equations are coupled by the standard kinematic and kinetic interface conditions, namely, continuity of displacements and forces. We propose a second-order pure-Lagrangian method combined with finite element approximations for the numerical solution of this problem. For this purpose, we use the mathematical formalism of continuum mechanics (see for instance [14]) following the ideas given in [4] and [2]. More precisely, the Navier-Stokes equations and the Navier-Lamé equations are written in material coordinates and in terms of displacements and fluid pressure. This new strategy avoids several difficulties presented by literature methods as some of those referenced above. For example, at each time step the computational domain is known and the problem to solve is linear. Moreover, the interface kinematic condition is included in the definition of the functional space where the numerical solution is looked for and the kinetic condition is a natural one of the weak formulation for the coupled fluid-solid problem.

The paper is organized as follows. In Section 2 a general initial-boundary value problem is posed in a time dependent bounded domain and some hypotheses and notations concerning motions are recalled. In Section 3, a change of variable from the current configuration to the initial configuration is proposed

obtaining a new strong formulation of the problem in a time-independent domain. More precisely, the fluid-structure interaction problem is written in Lagrangian coordinates and in terms of displacements and fluid pressure. Then, the standard associated weak problem is obtained. In Section 4, we propose a second-order time discretization scheme for solving the coupled weak formulation. Section 5 discusses the fully discretized scheme using a finite element method: in the solid, continuous piecewise linear functions are used for each component of the displacement field and, in the fluid, the same approximation for the pressure and the mini-element (P_1-bubble) for the displacement field. Moreover, we obtain approximations of velocity and pressure in Eulerian coordinates (i.e., in the current configuration) by using the obtained approximations of displacement and pressure in Lagrangian coordinates. A method to re-initialize the pure Lagrange-Galerkin method is presented in Section 6. Finally, in Section 7 numerical examples are included showing the performance of the overall method.

2. Statement of the problem. General assumptions and notations. Let Ω be a bounded domain in $\mathbb{R}^d$ ($d = 2, 3$) with Lipschitz boundary Γ. Let us assume that Ω and Γ are divided into two parts: $\Omega = int(\overline{\Omega}^f \cup \overline{\Omega}^s)$ and $\Gamma = \Gamma^D \cup \Gamma^N$, with $\Gamma^D \cap \Gamma^N = \emptyset$. We call $\Gamma^I = \overline{\Omega}^f \cap \overline{\Omega}^s$. Let $\mathbf{X} : \overline{\Omega} \times \mathbb{R} \longrightarrow \mathbb{R}^d$ be a *motion* in the sense of Gurtin [14]. For given $\mathcal{A} \subset \overline{\Omega}$, we call $\mathcal{A}_t = \mathbf{X}(\mathcal{A}, t)$. In practice, a bounded time interval is considered for the motion, namely, $[t_0, t_f]$, being t_0, t_f two non-negative numbers. For simplicity, in this paper we assume that $\mathbf{X}(\mathbf{p}, t_0) = \mathbf{p}\ \forall \mathbf{p} \in \overline{\Omega}$. Notice that in many cases the body is at rest until the initial time, i.e., $\mathbf{X}(\mathbf{p}, t) = \mathbf{p}\ \forall t \leq t_0\ \forall \mathbf{p} \in \overline{\Omega}$ and then the initial velocity is null. For given $t_0 \leq \tau \leq t_f$, we denote by $\mathbf{X}_\tau$ the motion relative to the configuration at time τ, namely

$$\mathbf{X}_\tau(\mathbf{y}, t) := \mathbf{X}(\mathbf{P}(\mathbf{y}, \tau), t) \quad \forall (\mathbf{y}, t) \in \overline{\Omega}_\tau \times [t_0, t_f]. \tag{2.1}$$

Let us introduce the notation

$$\mathbf{F}_\tau(\mathbf{y}, t) := \operatorname{grad}_{\mathbf{y}} \mathbf{X}_\tau(\mathbf{y}, t). \tag{2.2}$$

We will adopt the notation given in [2] for the trajectory of the motion ($\mathcal{T}$), the spatial velocity ($\mathbf{v}$), the displacement ($\mathbf{u}$), the deformation gradient ($\mathbf{F}$), the reference map ($\mathbf{P}$), the points in $\overline{\Omega}$ ($\mathbf{p}$), the points in $\overline{\Omega}_t$ ($\mathbf{x}$), the points in $\overline{\Omega}_\tau$ ($\mathbf{y}$), and the functional spaces involved in the formulation of the problem (see Section 2 of [2] for more details). Fields defined in $\mathcal{T}$ (respectively, in $\overline{\Omega} \times [t_0, t_f]$) are called *spatial fields* (respectively, *material fields*). For the sake of clarity, in expressions involving space and time derivatives we use the definitions and notations given in [14]. In particular, if Φ is a smooth material field, we denote by $\nabla\Phi$ (respectively, by $\operatorname{Div}\Phi$) the gradient (respectively, the divergence) with respect to the first argument ($\mathbf{p}$), and by $\dot{\Phi}$ the partial derivative with respect to the second argument (time). Similarly, if Ψ is a smooth spatial field or a smooth field defined in $\overline{\Omega}_\tau \times [t_0, t_f]$, we denote by $\operatorname{grad}\Psi$ (respectively, by $\operatorname{div}\Psi$) the gradient (respectively, the divergence) with respect to the first argument ($\mathbf{x}$ or $\mathbf{y}$), and by Ψ' the partial derivative with respect to the second argument (time). For the sake of clarity, in some places where these operators appear, we specify the differentiation variable as a subscript, e.g., $\nabla_{\mathbf{p}}\Phi$, $\operatorname{grad}_{\mathbf{x}}\Psi$, $\operatorname{grad}_{\mathbf{y}}\Psi$ (respectively, $\operatorname{Div}_{\mathbf{p}}\Phi$, $\operatorname{div}_{\mathbf{x}}\Psi$, $\operatorname{div}_{\mathbf{y}}\Psi$) denote the gradient (respectively, the divergence) with respect to the first argument ($\mathbf{p}$, $\mathbf{x}$ or $\mathbf{y}$). Moreover, if Ψ is a spatial field, $\dot{\Psi}$ denotes the *material time*

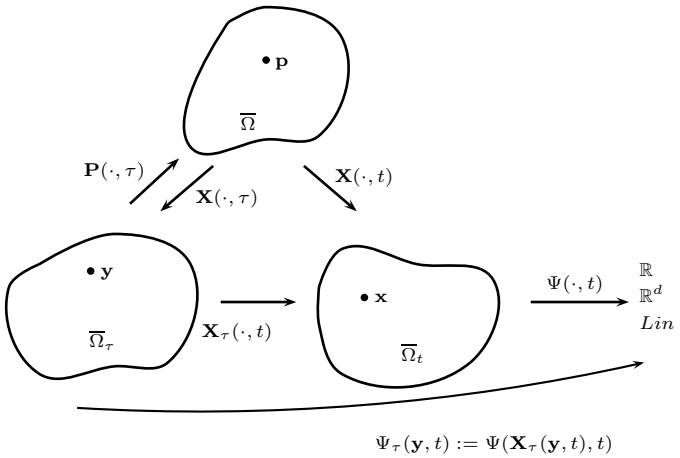

FIG. 2.1. *Functions referred to configuration at time τ, $t_0 \leq \tau \leq t_f$.*

derivative, that is $\dot{\Psi}(\mathbf{x}, t) = \dfrac{\partial}{\partial t}\left(\Psi(\mathbf{X}(\mathbf{p}, t), t)\right)_{|\mathbf{p}=\mathbf{P}(\mathbf{x},t)}$. Let us introduce the following definition of the

trajectory of the fluid motion (see [14]):

$$\mathcal{T}^f := \{(\mathbf{x},t) : \mathbf{x} \in \overline{\Omega}_t^f,\ t \in [t_0,t_f]\}.$$

A spatial field Ψ can also be defined in $\overline{\Omega}_\tau \times [t_0,t_f]$. It is the field

$$\Psi_\tau(\mathbf{y},t) := \Psi(\mathbf{X}_\tau(\mathbf{y},t),t) \quad \forall (\mathbf{y},t) \in \overline{\Omega}_\tau \times [t_0,t_f]. \tag{2.3}$$

These functions are depicted in Figure 2.1. For $\tau = t_0$, Ψ_{t_0} is the *material description* of Ψ also denoted by Ψ_m. Let $\mathbf{u}_\tau$ be the displacement field relative to the configuration at time τ, that is,

$$\mathbf{u}_\tau(\mathbf{y},t) := \mathbf{X}_\tau(\mathbf{y},t) - \mathbf{y} \quad \forall (\mathbf{y},t) \in \overline{\Omega}_\tau \times [t_0,t_f]. \tag{2.4}$$

Now, let us consider the following general initial-boundary value problem (motion equation of continuum mechanics):

(**GSP**) **General Strong Problem**. *Find two mappings* $\mathbf{v} : \mathcal{T} \longrightarrow \mathbb{R}^d$ *and* $\mathbf{T} : \mathcal{T} \longrightarrow Lin$ *such that*

$$\rho \mathbf{v}' + \rho \operatorname{grad} \mathbf{v}\mathbf{v} - \operatorname{div} \mathbf{T} = \mathbf{b} \text{ in } \mathcal{T}, \tag{2.5}$$

subject to the boundary conditions

$$\mathbf{v}(\mathbf{x},t) = \mathbf{v}_D(\mathbf{x},t) \text{ on } \Gamma_t^D, \tag{2.6}$$

$$\mathbf{T}(\mathbf{x},t)\mathbf{n}(\mathbf{x},t) = \mathbf{h}(\mathbf{x},t) \text{ on } \Gamma_t^N, \tag{2.7}$$

for $t \in (t_0,t_f)$*, and to the initial condition*

$$\mathbf{v}(\mathbf{x},t_0) = \mathbf{v}^0(\mathbf{x}) \text{ in } \overline{\Omega}. \tag{2.8}$$

In the above equations, *Lin* denotes the space of tensors in the d-dimensional space, $\rho : \mathcal{T} \longrightarrow \mathbb{R}$, $\mathbf{b} : \mathcal{T} \longrightarrow \mathbb{R}^d$, $\mathbf{v}_D(\cdot,t) : \Gamma_t^D \longrightarrow \mathbb{R}^d$ and $\mathbf{h}(\cdot,t) : \Gamma_t^N \longrightarrow \mathbb{R}^d$, $t \in (t_0,t_f)$, are given spatial fields, $\mathbf{n}(\cdot,t)$ is the outward unit normal vector to Γ_t. Notice that the system of equations given in (**GSP**) is undetermined. In Section 3, in order to complete the system, constitutive assumptions on the form of the Cauchy stress tensor $\mathbf{T}$ will be introduced. These additional equations depend on the behavior of the specific materials we are considering (e.g., fluid or solid). Moreover, we notice that equations (2.5)-(2.7) are expressed in spatial coordinates, $\mathbf{x} = \mathbf{X}(\mathbf{p},t)$, belonging, in general, to an unknown domain. In order to avoid this difficulty we will rewrite problem (**GSP**) in the reference configuration $\overline{\Omega}$ which is supposed to be given.

3. Strong problem and weak formulation in Lagrangian coordinates. We are going to develop some formal computations in order to write the above problem (**GSP**) in Lagrangian coordinates and in terms of displacement. Firstly, from the definition of the material time derivative and by using the chain rule, we get (see, for instance, [14])

$$\dot{\mathbf{v}}(\mathbf{x},t) = \frac{\partial \mathbf{v}}{\partial t}(\mathbf{x},t) + \operatorname{grad}_{\mathbf{x}} \mathbf{v}(\mathbf{x},t)\mathbf{v}(\mathbf{x},t) = \ddot{\mathbf{u}}(\mathbf{p},t)_{|\mathbf{p}=\mathbf{P}(\mathbf{x},t)} \ \forall (\mathbf{x},t) \in \mathcal{T}. \tag{3.1}$$

Then, by evaluating equation (2.5) at point $\mathbf{x} = \mathbf{X}(\mathbf{p},t)$ and then using (3.1), we obtain

$$\rho(\mathbf{X}(\mathbf{p},t),t)\ddot{\mathbf{u}}(\mathbf{p},t) - \operatorname{div}_{\mathbf{x}} \mathbf{T}(\mathbf{X}(\mathbf{p},t),t) = \mathbf{b}(\mathbf{X}(\mathbf{p},t),t), \tag{3.2}$$

for $(\mathbf{p},t) \in \Omega \times (t_0,t_f)$. Notice that in (3.2) there are derivatives with respect to the Eulerian variable $\mathbf{x}$. In order to write a strong formulation of problem (**GSP**) in Lagrangian coordinates we can use the divergence theorem, the change of variable $\mathbf{x} = \mathbf{X}(\mathbf{p},t)$, the chain rule and the localization theorem, to obtain the equality

$$-\operatorname{div}_{\mathbf{x}} \mathbf{T}(\mathbf{X}(\mathbf{p},t),t) = -\operatorname{Div}_{\mathbf{p}} \left(\mathbf{T}_m(\mathbf{p},t) \det \mathbf{F}(\mathbf{p},t) \mathbf{F}^{-t}(\mathbf{p},t)\right) \frac{1}{\det \mathbf{F}(\mathbf{p},t)}, \tag{3.3}$$

for $(\mathbf{p},t) \in \Omega \times (t_0,t_f)$. Then, (3.2) becomes

$$\rho_m \ddot{\mathbf{u}} - \frac{1}{\det \mathbf{F}} \operatorname{Div}_{\mathbf{p}} \left(\mathbf{T}_m \det \mathbf{F} \mathbf{F}^{-t}\right) = \mathbf{b}_m, \tag{3.4}$$

in $\Omega \times (t_0, t_f)$. Next, by evaluating equations (2.6) and (2.7) at point $\mathbf{x} = \mathbf{X}(\mathbf{p}, t)$ and using (2.8), we obtain the following material versions of the boundary and initial conditions:

$$\dot{\mathbf{u}} = (\mathbf{v}_D)_m \text{ on } \Gamma^D \times (t_0, t_f), \tag{3.5}$$

$$\mathbf{T}_m \mathbf{F}^{-t} \mathbf{m} = |\mathbf{F}^{-t} \mathbf{m}| \mathbf{h}_m \text{ on } \Gamma^N \times (t_0, t_f), \tag{3.6}$$

$$\dot{\mathbf{u}}(\mathbf{p}, t_0) = \mathbf{v}^0(\mathbf{p}) \text{ in } \overline{\Omega}, \tag{3.7}$$

being $\mathbf{m}$ the outward unit normal vector to Γ , and where we have used

$$\mathbf{n}(\mathbf{X}(\mathbf{p}, t), t) = \frac{\mathbf{F}^{-t}(\mathbf{p}, t)\mathbf{m}(\mathbf{p})}{|\mathbf{F}^{-t}(\mathbf{p}, t)\mathbf{m}(\mathbf{p})|} \quad (\mathbf{p}, t) \in \Gamma \times (t_0, t_f).$$

As a consequence of these results, equations of problem (**GSP**) in the current configuration are transformed into equations in the reference configuration $\overline{\Omega}$. More precisely, we have got the following formulation in $\Omega \times (t_0, t_f)$:

(**LGSP**) **Lagrangian General Strong Problem**. *Find two functions* $\mathbf{u} : \overline{\Omega} \times [t_0, t_f] \longrightarrow \mathbb{R}^d$ *and* $\mathbf{T}_m : \overline{\Omega} \times [t_0, t_f] \longrightarrow$ *Lin satisfying (3.4), subject to boundary conditions (3.5) and (3.6), and to initial condition (3.7).*

Although the numerical method could be written for a more general case, for simplicity of this presentation, we are going to consider two specific types of materials in the domain Ω. More precisely, at each instant $t \in [t_0, t_f]$, let us consider an incompressible Newtonian fluid occupying domain Ω_t^f and a homogeneous isotropic linear elastic material occupying domain Ω_t^s. Moreover, let us also assume, for the sake of simplicity, that *the residual stress* in the solid is null, i.e., $\mathbf{T}(\mathbf{p}, t_0) = \mathbf{0}\ \forall \mathbf{p} \in \Omega^s$. Next, we recall the constitutive equations for these materials:

- For an incompressible Newtonian fluid, the Cauchy stress tensor $\mathbf{T}$ has the following form:

$$\mathbf{T} = -\pi \mathbf{I} + \eta(\operatorname{grad} \mathbf{v} + \operatorname{grad} \mathbf{v}^t) \text{ in } \mathcal{T}^f \tag{3.8}$$

  In the above equation, $\pi : \mathcal{T}^f \longrightarrow \mathbb{R}$ denotes the pressure (unknown) and η the dynamic viscosity (known). Motion equation (3.4) must be supplemented by the constitutive equation (3.8) and the incompressibility condition

$$\operatorname{div} \mathbf{v} = 0 \text{ in } \mathcal{T}^f \tag{3.9}$$

- For a homogeneous isotropic linear elastic material, *the first Piola-Kirchoff stress tensor*:

$$\mathbf{T}_m \det \mathbf{F} \mathbf{F}^{-t},$$

  is related with displacement by the approximate equality (see, for instance, [14])

$$\mathbf{T}_m \det \mathbf{F} \mathbf{F}^{-t} \simeq \lambda \operatorname{Div} \mathbf{u} \mathbf{I} + 2\mu \mathcal{E}(\mathbf{u}) \text{ in } \Omega^s \times (t_0, t_f), \tag{3.10}$$

  where λ and μ are the Lamé coefficients and $\mathcal{E}(\mathbf{u}) = 1/2\left(\nabla \mathbf{u} + \nabla \mathbf{u}^t\right)$ is the *infinitesimal strain tensor* (see for instance [14]). Let us recall that the Lamé coefficients can be written in terms of Young modulus E and Poisson ratio ν as follows:

$$\mu = \frac{E}{2(1+\nu)}, \quad \lambda = \frac{E\nu}{(1+\nu)(1-2\nu)}.$$

Similar to the motion equation, we write equations (3.8) and (3.9) in Lagrangian coordinates. Firstly, by using the chain rule, we obtain (see, for instance, [14])

$$\begin{aligned} \operatorname{div}_{\mathbf{x}} \mathbf{v}(\mathbf{X}(\mathbf{p}, t), t) &= \operatorname{tr}(\operatorname{grad}_{\mathbf{x}} \mathbf{v}(\mathbf{X}(\mathbf{p}, t), t)) = \operatorname{tr}\left(\nabla \dot{\mathbf{u}}(\mathbf{p}, t) \mathbf{F}^{-1}(\mathbf{p}, t)\right) \\ &= \nabla \dot{\mathbf{u}}(\mathbf{p}, t) \mathbf{F}^{-1}(\mathbf{p}, t) \cdot \mathbf{I} = \nabla \dot{\mathbf{u}}(\mathbf{p}, t) \cdot \mathbf{F}^{-t}(\mathbf{p}, t)\ \forall (\mathbf{p}, t) \in \Omega^f \times (t_0, t_f). \end{aligned} \tag{3.11}$$

Next, by evaluating equations (3.8) and (3.9) at point $\mathbf{x} = \mathbf{X}(\mathbf{p}, t)$, using the chain rule in (3.8), and equality (3.11), we get

$$\mathbf{T}_m = -\pi_m \mathbf{I} + \eta\left(\nabla \dot{\mathbf{u}} \mathbf{F}^{-1} + \mathbf{F}^{-t}(\nabla \dot{\mathbf{u}})^t\right) \text{ in } \Omega^f \times (t_0, t_f), \tag{3.12}$$

$$\nabla \dot{\mathbf{u}} \cdot \mathbf{F}^{-t} = 0 \text{ in } \Omega^f \times (t_0, t_f), \tag{3.13}$$

Let us introduce equations (3.10), (3.12) and (3.13) in the above problem. Then, we have the following fluid-structure interaction problem written in the reference configuration:

(**LFSP**) **Lagrangian fluid-structure interaction problem**. *Find two functions* $\mathbf{u} : \overline{\Omega}\times[t_0,t_f] \longrightarrow \mathbb{R}^d$ *and* $\pi_m : \overline{\Omega}^f \times [t_0,t_f] \longrightarrow \mathbb{R}$ *such that*

$$\rho_m\ddot{\mathbf{u}} - \frac{1}{\det\mathbf{F}}\,\mathrm{Div}\,\left(\mathbf{T}_m \det\mathbf{F}\mathbf{F}^{-t}\right) = \mathbf{b}_m \ \textit{in}\ \Omega\times(t_0,t_f), \tag{3.14}$$

$$\mathbf{T}_m = -\pi_m\mathbf{I} + \eta\left(\nabla\dot{\mathbf{u}}\mathbf{F}^{-1} + \mathbf{F}^{-t}\left(\nabla\dot{\mathbf{u}}\right)^t\right) \ \textit{in}\ \Omega^f\times(t_0,t_f), \tag{3.15}$$

$$\nabla\dot{\mathbf{u}}\cdot\mathbf{F}^{-t} = 0 \ \textit{in}\ \Omega^f\times(t_0,t_f), \tag{3.16}$$

$$\mathbf{T}_m \det\mathbf{F}\mathbf{F}^{-t} = \lambda\,\mathrm{Div}\,\mathbf{u}\mathbf{I} + 2\mu\mathcal{E}(\mathbf{u}) \ \textit{in}\ \Omega^s\times(t_0,t_f), \tag{3.17}$$

subject to the boundary conditions

$$\dot{\mathbf{u}} = (\mathbf{v}_D)_m \ \textit{on}\ \Gamma^D\times(t_0,t_f), \tag{3.18}$$

$$\mathbf{T}_m\mathbf{F}^{-t}\mathbf{m} = |\mathbf{F}^{-t}\mathbf{m}|\mathbf{h}_m \ \textit{on}\ \Gamma^N\times(t_0,t_f), \tag{3.19}$$

and to the initial condition

$$\dot{\mathbf{u}}(\mathbf{p},t_0) = \mathbf{v}^0(\mathbf{p}) \ \textit{in}\ \overline{\Omega}. \tag{3.20}$$

Now, by multiplying equation (3.14) by $\det\mathbf{F}$ and by a test function $\mathbf{z}\in\mathbf{H}^1_{\Gamma^D}(\Omega)$, integrating in Ω, applying the usual Green's formula and equations (3.15), (3.17) and (3.19) we easily get a weak formulation for the motion equation. Similarly, by multiplying equation (3.16) by $\det\mathbf{F}$ and by a test function $q\in L^2(\Omega^f)$ and integrating in Ω^f we obtain a weak formulation for the incompressibility equation in the fluid. The whole problem is the following:

$$\begin{aligned}
\int_\Omega \rho_m \det\mathbf{F}\ddot{\mathbf{u}}\cdot\mathbf{z}\,d\mathbf{p} - \int_{\Omega^f}\pi_m\det\mathbf{F}\mathbf{F}^{-t}\cdot\nabla\mathbf{z}\,d\mathbf{p}\\
+\eta\int_{\Omega^f}\left(\nabla\dot{\mathbf{u}}\mathbf{F}^{-1}+\mathbf{F}^{-t}\left(\nabla\dot{\mathbf{u}}\right)^t\right)\det\mathbf{F}\mathbf{F}^{-t}\cdot\nabla\mathbf{z}\,d\mathbf{p} + \lambda\int_{\Omega^s}\mathrm{Div}\,\mathbf{u}\,\mathrm{Div}\,\mathbf{z}\,d\mathbf{p}\\
+2\mu\int_{\Omega^s}\mathcal{E}(\mathbf{u})\cdot\mathcal{E}(\mathbf{z})\,d\mathbf{p} = \int_\Omega\mathbf{b}_m\cdot\mathbf{z}\det\mathbf{F}\,d\mathbf{p} + \int_{\Gamma^N}|\mathbf{F}^{-t}\mathbf{m}|\det\mathbf{F}\mathbf{h}_m\cdot\mathbf{z}\,dA_\mathbf{p},
\end{aligned} \tag{3.21}$$

$$\int_{\Omega^f}\det\mathbf{F}\nabla\dot{\mathbf{u}}\cdot\mathbf{F}^{-t}q\,d\mathbf{p} = 0, \tag{3.22}$$

$\forall\mathbf{z}\in\mathbf{H}^1_{\Gamma^D}(\Omega)$ and $\forall q\in L^2(\Omega^f)$. Notice that the above problem is non-linear in the fluid but not in the solid. However, extension of what follows to nonlinear solids is straightforward. Moreover, let us notice that fluid-solid coupling is implicitely included. More precisely, continuity of displacements across the interface is included in the function space where the solution is looked for (essential condition) while the kinetic condition is a natural condition for (3.21).

Numerical methods applied to formulations in material coordinates are called pure-Lagrangian methods. Thus, from (3.21)-(3.22), we can obtain different pure-Lagrangian numerical methods. These methods are useful, in particular, for solving free surface problems because the computational domain is independent of time.

Remark 3.1. Notice that in equations (3.21)-(3.22), the integrals corresponding to the fluid can also be written in terms of the velocity instead of the displacement, by replacing $\dot{\mathbf{u}}$ with $\mathbf{v}_m$. Thus, from (3.21)-(3.22) we can obtain pure-Lagrangian methods whose unknowns are either the fluid velocity, the fluid pressure and the solid displacement, or the fluid and solid displacements and the fluid pressure. We will call the latter a displacement method. In this paper, we propose a second-order pure-Lagrangian displacement method.

4. Time discretization. Depending on the differentiation formulas used to approximate the time derivatives, we can obtain, from (3.21)-(3.22), different pure-Lagrangian methods. In this section, we introduce a Newmark-like second-order centered scheme for time semi-discretization of (3.21)-(3.22).

The following notations will be used in the rest of the paper. Let us denote the number of time steps by N, the time step $\Delta t = (T-t_0)/N$, and the mesh-points $t_n = t_0 + n\Delta t$. We will use the notation

$\Psi^l(\mathbf{y}) := \Psi(\mathbf{y}, t_l)$ for a function $\Psi(\mathbf{y}, t)$. Similarly, for a given material field Φ (respectively, a spatial field Ψ) we will denote by $\Phi^l_{\Delta t}$ (respectively, $\Psi^l_{m,\Delta t}$) approximations of Φ^l (respectively, Ψ^l_m) obtained with a time-semidiscretized scheme.

In order to discretize the time derivatives $\ddot{\mathbf{u}}$ and $\dot{\mathbf{u}}$ in equations (3.21)-(3.22), we propose the following second-order centered formulas:

- Three-points:

$$\frac{\partial^2 \Psi}{\partial t^2}(\mathbf{y}, t) = \frac{\Psi(\mathbf{y}, t + \Delta t) - 2\Psi(\mathbf{y}, t) + \Psi(\mathbf{y}, t - \Delta t)}{\Delta t^2} + O(\Delta t^2). \tag{4.1}$$

- Two-points:

$$\frac{\partial \Psi}{\partial t}(\mathbf{y}, t) = \frac{\Psi(\mathbf{y}, t + \Delta t) - \Psi(\mathbf{y}, t - \Delta t)}{2\Delta t} + O(\Delta t^2). \tag{4.2}$$

Moreover, the following interpolation formula will be convenient to approximate the gradient of the solid displacement:

$$\operatorname{grad} \Psi(\mathbf{y}, t) = \frac{\operatorname{grad} \Psi(\mathbf{y}, t + \Delta t) + \operatorname{grad} \Psi(\mathbf{y}, t - \Delta t)}{2} + O(\Delta t^2). \tag{4.3}$$

Then, by evaluating (3.21) and (3.22) at time $t = t_{n+1/2}$ and then using second-order formulas (4.1), (4.2) and (4.3) for $\Psi = \mathbf{u}$, we deduce the following Newmark-like time-semidiscretized scheme:

$$\begin{aligned}
&\int_\Omega \rho^{n+1/2} \circ \mathbf{X}^{n+1/2}_{\Delta t} \det \mathbf{F}^{n+1/2}_{\Delta t} \frac{\mathbf{u}^{n+3/2}_{\Delta t} - 2\mathbf{u}^{n+1/2}_{\Delta t} + \mathbf{u}^{n-1/2}_{\Delta t}}{\Delta t^2} \cdot \mathbf{z}\, d\mathbf{p} \\
&\quad - \int_{\Omega^f} \pi^{n+1/2}_{m,\Delta t} \det \mathbf{F}^{n+1/2}_{\Delta t} (\mathbf{F}^{n+1/2}_{\Delta t})^{-t} \cdot \nabla \mathbf{z}\, d\mathbf{p} \\
&\quad + \eta \int_{\Omega^f} \det \mathbf{F}^{n+1/2}_{\Delta t} \frac{\nabla \mathbf{u}^{n+3/2}_{\Delta t} - \nabla \mathbf{u}^{n-1/2}_{\Delta t}}{2\Delta t} (\mathbf{F}^{n+1/2}_{\Delta t})^{-1} (\mathbf{F}^{n+1/2}_{\Delta t})^{-t} \cdot \nabla \mathbf{z}\, d\mathbf{p} \\
&\quad + \eta \int_{\Omega^f} \det \mathbf{F}^{n+1/2}_{\Delta t} (\mathbf{F}^{n+1/2}_{\Delta t})^{-t} \frac{(\nabla \mathbf{u}^{n+3/2}_{\Delta t})^t - (\nabla \mathbf{u}^{n-1/2}_{\Delta t})^t}{2\Delta t} (\mathbf{F}^{n+1/2}_{\Delta t})^{-t} \cdot \nabla \mathbf{z}\, d\mathbf{p} \\
&\quad + \frac{\lambda}{2} \int_{\Omega^s} \left(\operatorname{Div} \mathbf{u}^{n+3/2}_{\Delta t} + \operatorname{Div} \mathbf{u}^{n-1/2}_{\Delta t} \right) \operatorname{Div} \mathbf{z}\, d\mathbf{p} + \mu \int_{\Omega^s} \left(\mathcal{E}(\mathbf{u}^{n+3/2}_{\Delta t}) + \mathcal{E}(\mathbf{u}^{n-1/2}_{\Delta t}) \right) \cdot \mathcal{E}(\mathbf{z})\, d\mathbf{p} \\
&= \int_\Omega \mathbf{b}^{n+1/2} \circ \mathbf{X}^{n+1/2}_{\Delta t} \cdot \mathbf{z} \det \mathbf{F}^{n+1/2}_{\Delta t}\, d\mathbf{p} + \int_{\Gamma^N} |(\mathbf{F}^{n+1/2}_{\Delta t})^{-t} \mathbf{m}| \det \mathbf{F}^{n+1/2}_{\Delta t} \mathbf{h}^{n+1/2} \circ \mathbf{X}^{n+1/2}_{\Delta t} \cdot \mathbf{z}\, dA_{\mathbf{p}}, \quad (4.4) \\
&\int_{\Omega^f} \det \mathbf{F}^{n+1/2}_{\Delta t} \frac{\nabla \mathbf{u}^{n+3/2}_{\Delta t} - \nabla \mathbf{u}^{n-1/2}_{\Delta t}}{2\Delta t} \cdot (\mathbf{F}^{n+1/2}_{\Delta t})^{-t} q\, d\mathbf{p} = 0, \quad (4.5)
\end{aligned}$$

$\forall \mathbf{z} \in \mathbf{H}^1_{\Gamma^D}(\Omega)$, $\forall q \in L^2(\Omega^f)$ and $0 \le n \le N-1$. Notice that $\mathbf{X}$ and $\mathbf{F}$ appearing in equations (3.21) and (3.22) are unknown. However, they can be easily approximated from $\mathbf{u}$ by using the following equalities:

$$\begin{aligned}
\mathbf{X}(\mathbf{p}, t) &= \mathbf{p} + \mathbf{u}(\mathbf{p}, t), \\
\mathbf{F}(\mathbf{p}, t) &= \nabla \mathbf{X}(\mathbf{p}, t) = \mathbf{I} + \nabla \mathbf{u}(\mathbf{p}, t),
\end{aligned}$$

for $(\mathbf{p}, t) \in \Omega \times (t_0, t_f)$. More precisely, in the above pure-Lagrangian scheme we have used the following approximations of $\mathbf{X}^{n+1/2}$ and $\mathbf{F}^{n+1/2}$:

$$\begin{aligned}
\mathbf{X}^{n+1/2}_{\Delta t}(\mathbf{p}) &:= \mathbf{p} + \mathbf{u}^{n+1/2}_{\Delta t}(\mathbf{p}), \\
\mathbf{F}^{n+1/2}_{\Delta t}(\mathbf{p}) &:= \mathbf{I} + \nabla \mathbf{u}^{n+1/2}_{\Delta t}(\mathbf{p}),
\end{aligned}$$

for $\mathbf{p} \in \Omega$ and $0 \le n \le N-1$. Let us emphasize that while the continuous problem is non-linear, *the implicit semi-discrete scheme (4.4)-(4.5) is linear* in the two unknowns $\mathbf{u}^{n+3/2}_{\Delta t}$ and $\pi^{n+1/2}_{m,\Delta t}$. Moreover, we can easily see that the consistency error is of order two.

Remark 4.1. Let us observe that the initial condition $\mathbf{u}^{1/2}$ appearing in scheme (4.4)-(4.5) is unknown but it can be approximated by using the initial condition for the continuous problem (3.20). More precisely,

by using the following Taylor expansions satisfied by a smooth enough displacement field

$$\mathbf{u}(\mathbf{p},t-\Delta t/2)=\mathbf{u}(\mathbf{p},t)-\mathbf{v}_m(\mathbf{p},t)\frac{\Delta t}{2}+\dot{\mathbf{v}}(\mathbf{X}(\mathbf{p},t),t)\frac{\Delta t^2}{8}+O(\Delta t^3), \tag{4.6}$$

$$\mathbf{u}(\mathbf{p},t+\Delta t/2)=\mathbf{u}(\mathbf{p},t)+\mathbf{v}_m(\mathbf{p},t)\frac{\Delta t}{2}+\dot{\mathbf{v}}(\mathbf{X}(\mathbf{p},t),t)\frac{\Delta t^2}{8}+O(\Delta t^3), \tag{4.7}$$

we deduce a third-order approximation of $\mathbf{u}^{1/2}$, namely,

$$\mathbf{u}_{\Delta t}^{1/2}:=\mathbf{u}^{-1/2}+\mathbf{v}^0\Delta t \text{ in } \overline{\Omega}. \tag{4.8}$$

For simplicity, let us assume that initial velocity $\mathbf{v}^0$ is null so we take

$$\mathbf{u}_{\Delta t}^{-1/2}=\mathbf{u}_{\Delta t}^{1/2}=\mathbf{0} \text{ in } \overline{\Omega}. \tag{4.9}$$

Otherwise, it is convenient to write the considered problem in configuration $\overline{\Omega}_{t_0-\Delta t/2}$ instead of $\overline{\Omega}$ noting that $\mathbf{u}_{t_0-\Delta t/2}^{-1/2}\equiv\mathbf{0}$ (see [2] for details). In the academic test examples considered in this paper, the initial velocity is not null but we know and use the exact value of $\mathbf{u}^{-1/2}$. We have observed quite surprisingly that if we start with a third order approximation of displacement $\mathbf{u}^{1/2}$ as (4.8), then the above method is also second-order accurate not only for displacements but for the velocity as well. In order to understand the reason of this fact, we are going to analyze the following simple scheme

$$\frac{\mathbf{u}_{\Delta t}^{n+3/2}-2\mathbf{u}_{\Delta t}^{n+1/2}+\mathbf{u}_{\Delta t}^{n-1/2}}{\Delta t^2}=\ddot{\mathbf{u}}^{n+1/2} \text{ in } \overline{\Omega}, \tag{4.10}$$

for $0\leq n\leq N-1$. If $\mathbf{u}$ is smooth enough, we have

$$\frac{\mathbf{u}^{n+3/2}-2\mathbf{u}^{n+1/2}+\mathbf{u}^{n-1/2}}{\Delta t^2}=\ddot{\mathbf{u}}^{n+1/2}+O(\Delta t^2) \text{ in } \overline{\Omega}, \tag{4.11}$$

for $0\leq n\leq N-1$. By subtracting (4.11) from (4.10) we get

$$\begin{aligned}&\frac{\mathbf{u}_{\Delta t}^{n+3/2}-\mathbf{u}_{\Delta t}^{n+1/2}}{\Delta t^2}-\frac{\mathbf{u}_{\Delta t}^{n+1/2}-\mathbf{u}_{\Delta t}^{n-1/2}}{\Delta t^2}\\ &=\frac{\mathbf{u}^{n+3/2}-\mathbf{u}^{n+1/2}}{\Delta t^2}-\frac{\mathbf{u}^{n+1/2}-\mathbf{u}^{n-1/2}}{\Delta t^2}+O(\Delta t^2) \text{ in } \overline{\Omega},\end{aligned} \tag{4.12}$$

for $0\leq n\leq N-1$. Now, for fixed q, $0\leq q\leq N-1$, let us add (4.12) multiplied by Δt from $n=0$ to $n=q$. We have

$$\begin{aligned}&\frac{\mathbf{u}_{\Delta t}^{q+3/2}-\mathbf{u}_{\Delta t}^{q+1/2}}{\Delta t}-\frac{\mathbf{u}^{q+3/2}-\mathbf{u}^{q+1/2}}{\Delta t}\\ &=\frac{\mathbf{u}_{\Delta t}^{1/2}-\mathbf{u}_{\Delta t}^{-1/2}}{\Delta t}-\frac{\mathbf{u}^{1/2}-\mathbf{u}^{-1/2}}{\Delta t}+O(\Delta t^2) \text{ in } \overline{\Omega}.\end{aligned} \tag{4.13}$$

Next, by subtracting (4.6) from (4.7) for $t=t_{q+1}$ and then using (4.13), we obtain

$$\frac{\mathbf{u}_{\Delta t}^{q+3/2}-\mathbf{u}_{\Delta t}^{q+1/2}}{\Delta t}-(\mathbf{v}_m)^{q+1}=\frac{\mathbf{u}_{\Delta t}^{1/2}-\mathbf{u}_{\Delta t}^{-1/2}}{\Delta t}-\frac{\mathbf{u}^{1/2}-\mathbf{u}^{-1/2}}{\Delta t}+O(\Delta t^2) \text{ in } \overline{\Omega}, \tag{4.14}$$

for $0\leq q\leq N-1$. Now, from this equality we deduce that, for the simple scheme (4.10), a second-order approximation of the material velocity is obtained if the initial conditions satisfy

$$\frac{\mathbf{u}_{\Delta t}^{1/2}-\mathbf{u}_{\Delta t}^{-1/2}}{\Delta t}-\frac{\mathbf{u}^{1/2}-\mathbf{u}^{-1/2}}{\Delta t}=O(\Delta t^2) \text{ in } \overline{\Omega}. \tag{4.15}$$

Therefore, for scheme (4.4)-(4.5) a second-order approximation for the velocity is obtained when we start with $\mathbf{u}_{\Delta t}^{-1/2}=\mathbf{u}^{-1/2}$ and $\mathbf{u}_{\Delta t}^{1/2}$ given in (4.8). Notice that if the displacement field is smooth enough, these initial conditions satisfy (4.15).

Remark 4.2. By using analogous procedures to the ones in the previous remark, we can obtain approximate Dirichlet boundary conditions for the displacement. More precisely, by using that

$$\mathbf{u}^{n+3/2} = \mathbf{u}^{n-1/2} + 2\Delta t \mathbf{v}^{n+1/2}\left(\mathbf{X}^{n+1/2}\right) + O(\Delta t^3),$$

we deduce the following Dirichlet boundary condition for $\mathbf{u}^{n+3/2}$ preserving the second order of the global scheme:

$$\mathbf{u}_{\Delta t}^{n+3/2} = \mathbf{u}_{\Delta t}^{n-1/2} + 2\Delta t \mathbf{v}_D^{n+1/2}\left(\mathbf{X}_{\Delta t}^{n+1/2}\right) \text{ on } \Gamma^D,$$

for $0 \leq n \leq N-1$.

5. Space discretization. Finite element method. In this section we propose a space discretization of the time semidiscretized problem (4.4)-(4.5) by using finite elements. More precisely, we consider continuous piecewise-linear for each solid displacement component and for the fluid the *mini-element* (see [1]), that is, continuous piecewise-linear+bubble finite element for each fluid displacement component and continuous piecewise-linear for pressure. In what follows, for a given material field Φ (respectively, a spatial field Ψ) we will denote by $\Phi^l_{\Delta t,h}$ (respectively, $\Psi^l_{m,\Delta t,h}$) approximations of Φ^l (respectively, Ψ^l_m) obtained with a fully discretized scheme, being h the meshsize.

Let us suppose Ω^f and Ω^s are two bounded domains in $\mathbb{R}^d$ with Lipschitz polygonal boundaries. Let us consider two suitable families of regular triangulations of $\overline{\Omega}^f$ and $\overline{\Omega}^s$ to be denoted by $\mathfrak{T}_h^f$ and $\mathfrak{T}_h^s$ respectively, both consisting of elements K of diameter $\leq h$. Moreover, let us assume they are compatible with the partition of the boundary of Ω into Γ^D and Γ^N and have the same vertices on the interface Γ^I for both fluid and solid (i.e., they are conformal meshes).

We define the following polynomial spaces:

$$P_1(K) = \left\{q_{|_K} \text{ with } q : \mathbb{R}^d \longrightarrow \mathbb{R} \text{ polynomial of degree } \leq 1\right\},$$
$$P_b(K) = \left\{q + \alpha\lambda_b^K : \ q \in P_1(K), \ \alpha \in \mathbb{R}\right\},$$

where λ_b^K is the bubble function of element K. We consider the following spaces of finite elements:

$$\mathbf{X}_h = \left\{\mathbf{w}_h \in \left(C^0(\overline{\Omega})\right)^d : \ \mathbf{w}_{h|_K} \in (P_b(K))^d \ \forall K \in \mathfrak{T}_h^f, \ \mathbf{w}_{h|_K} \in (P_1(K))^d \ \forall K \in \mathfrak{T}_h^s\right\}, \tag{5.1}$$

$$\mathbf{X}_{0h} = \left\{\mathbf{w}_h \in \mathbf{X}_h : \ \mathbf{w}_h = \mathbf{0} \text{ on } \Gamma^D\right\}, \tag{5.2}$$

$$V_h = \left\{\varphi_h \in C^0(\overline{\Omega}^f) : \ \varphi_{h|_K} \in P_1(K) \ \forall K \in \mathfrak{T}_h^f\right\}. \tag{5.3}$$

Let us notice that for the continuity through the fluid-solid interface it is enough that the displacement components coincide at the vertices on this interface because bubbles are null on the boundaries of the mesh elements. In order to obtain a fully discrete scheme of the time semi-discretized problem (4.4)-(4.5) we use spaces $\mathbf{X}_h$, $\mathbf{X}_{0h}$ and V_h to approximate function spaces $\mathbf{H}^1(\Omega)$, $\mathbf{H}^1_{\Gamma^D}(\Omega)$ and $L^2(\Omega^f)$, respectively. Thus, we obtain the following fully discrete problem:

(**LG**) **Pure Lagrange-Galerkin problem**. Find two sequences of functions $\widehat{\mathbf{u}}_{\Delta t,h} = \{\mathbf{u}_{\Delta t,h}^{n+3/2}\}_{n=0}^{N-1} \in [\mathbf{X}_h]^N$ and $\widehat{\pi}_{m,\Delta t,h} = \{\pi_{m,\Delta t,h}^{n+1/2}\}_{n=0}^{N-1} \in [V_h]^N$ such that

$$\begin{aligned}
&\int_\Omega \rho^{n+1/2} \circ \mathbf{X}_{\Delta t,h}^{n+1/2} \det \mathbf{F}_{\Delta t,h}^{n+1/2} \frac{\mathbf{u}_{\Delta t,h}^{n+3/2} - 2\mathbf{u}_{\Delta t,h}^{n+1/2} + \mathbf{u}_{\Delta t,h}^{n-1/2}}{\Delta t^2} \cdot \mathbf{z}_h \, d\mathbf{p} \\
&\qquad - \int_{\Omega^f} \pi_{m,\Delta t,h}^{n+1/2} \det \mathbf{F}_{\Delta t,h}^{n+1/2} (\mathbf{F}_{\Delta t,h}^{n+1/2})^{-t} \cdot \nabla \mathbf{z}_h \, d\mathbf{p} \\
&+\eta \int_{\Omega^f} \det \mathbf{F}_{\Delta t,h}^{n+1/2} \frac{\nabla \mathbf{u}_{\Delta t,h}^{n+3/2} - \nabla \mathbf{u}_{\Delta t,h}^{n-1/2}}{2\Delta t} (\mathbf{F}_{\Delta t,h}^{n+1/2})^{-1} (\mathbf{F}_{\Delta t,h}^{n+1/2})^{-t} \cdot \nabla \mathbf{z}_h \, d\mathbf{p} \\
&+\eta \int_{\Omega^f} \det \mathbf{F}_{\Delta t,h}^{n+1/2} (\mathbf{F}_{\Delta t,h}^{n+1/2})^{-t} \frac{(\nabla \mathbf{u}_{\Delta t,h}^{n+3/2})^t - (\nabla \mathbf{u}_{\Delta t,h}^{n-1/2})^t}{2\Delta t} (\mathbf{F}_{\Delta t,h}^{n+1/2})^{-t} \cdot \nabla \mathbf{z}_h \, d\mathbf{p} \\
&\qquad + \frac{\lambda}{2} \int_{\Omega^s} \left(\operatorname{Div} \mathbf{u}_{\Delta t,h}^{n+3/2} + \operatorname{Div} \mathbf{u}_{\Delta t,h}^{n-1/2}\right) \operatorname{Div} \mathbf{z}_h \, d\mathbf{p} \\
&+\mu \int_{\Omega^s} \left(\mathcal{E}(\mathbf{u}_{\Delta t,h}^{n+3/2}) + \mathcal{E}(\mathbf{u}_{\Delta t,h}^{n-1/2})\right) \cdot \mathcal{E}(\mathbf{z}_h) \, d\mathbf{p} = \int_\Omega \mathbf{b}^{n+1/2} \circ \mathbf{X}_{\Delta t,h}^{n+1/2} \cdot \mathbf{z}_h \det \mathbf{F}_{\Delta t,h}^{n+1/2} \, d\mathbf{p}
\end{aligned}$$

$$+\int_{\Gamma^N} |(\mathbf{F}_{\Delta t,h}^{n+1/2})^{-t}\mathbf{m}| \det \mathbf{F}_{\Delta t,h}^{n+1/2} \mathbf{h}^{n+1/2} \circ \mathbf{X}_{\Delta t,h}^{n+1/2} \cdot \mathbf{z}_h \, dA_{\mathbf{p}} \ \forall \mathbf{z}_h \in \mathbf{X}_{0h}, \tag{5.4}$$

$$\int_{\Omega^f} \det \mathbf{F}_{\Delta t,h}^{n+1/2} \frac{\nabla \mathbf{u}_{\Delta t,h}^{n+3/2} - \nabla \mathbf{u}_{\Delta t,h}^{n-1/2}}{2\Delta t} \cdot (\mathbf{F}_{\Delta t,h}^{n+1/2})^{-t} q_h \, d\mathbf{p} = 0 \ \forall q_h \in V_h, \tag{5.5}$$

for $0 \leq n \leq N-1$, subject to the initial and boundary conditions

$$\mathbf{u}_{\Delta t,h}^{-1/2}(\mathbf{p}) = \mathbf{u}^{-1/2}(\mathbf{p}) \text{ for all node } \mathbf{p} \text{ of mesh } \mathfrak{T}_h^f \cup \mathfrak{T}_h^s, \tag{5.6}$$

$$\mathbf{u}_{\Delta t,h}^{1/2}(\mathbf{p}) = \mathbf{u}_{\Delta t,h}^{-1/2}(\mathbf{p}) + \mathbf{v}^0(\mathbf{p})\Delta t \text{ for all node } \mathbf{p} \text{ of mesh } \mathfrak{T}_h^f \cup \mathfrak{T}_h^s, \tag{5.7}$$

$$\mathbf{u}_{\Delta t,h}^{n+3/2}(\mathbf{p}) = \mathbf{u}_{\Delta t,h}^{n-1/2}(\mathbf{p}) + 2\Delta t \mathbf{v}_D^{n+1/2}\left(\mathbf{X}_{\Delta t,h}^{n+1/2}(\mathbf{p})\right)$$
$$\text{for all node } \mathbf{p} \text{ of mesh } \mathfrak{T}_h^f \cup \mathfrak{T}_h^s \text{ on } \Gamma^D, \text{ and } 0 \leq n \leq N-1, \tag{5.8}$$

and where

$$\mathbf{X}_{\Delta t,h}^{n+1/2}(\mathbf{p}) := \mathbf{p} + \mathbf{u}_{\Delta t,h}^{n+1/2}(\mathbf{p}), \tag{5.9}$$

$$\mathbf{F}_{\Delta t,h|K}^{n+1/2} := \mathbf{I} + \nabla \mathbf{u}_{\Delta t,h|K}^{n+1/2}, \tag{5.10}$$

for $\mathbf{p} \in \overline{\Omega}$, $K \in \mathfrak{T}_h^f \cup \mathfrak{T}_h^s$ and $0 \leq n \leq N-1$. Notice that for displacement methods as the one above, the fluid-solid coupling at the interface is straightforward. In particular, the interface kinematic condition is included in the definition of the functional space where the solution is looked for.

By using the solution of problem (**LG**), we can obtain approximations of the followings fields: the material description of the velocity at times $\{t_{n+1}\}_{n=0}^{N-1}$, the motion at times $\{t_{n+1}\}_{n=0}^{N-1}$, the spatial description of the velocity at times $\{t_{n+1}\}_{n=0}^{N-1}$, the pressure in spatial coordinates at times $\{t_{n+1/2}\}_{n=0}^{N-1}$ and the stress tensor in spatial coordinates at times $\{t_{n+1/2}\}_{n=0}^{N-1}$. These approximations will be denoted respectively by $\{\mathbf{v}_{m,\Delta t,h}^{n+1}\}_{n=0}^{N-1}$, $\{\mathbf{X}_{\Delta t,h}^{n+1}\}_{n=0}^{N-1}$, $\{\mathbf{v}_{\Delta t,h}^{n+1}\}_{n=0}^{N-1}$, $\{\pi_{\Delta t,h}^{n+1/2}\}_{n=0}^{N-1}$ and $\{\mathbf{T}_{\Delta t,h}^{n+1/2}\}_{n=0}^{N-1}$. Moreover, we will denote by $\{\mathbf{p}_i^h\}_{i=1}^{N_v^h}$, $\{\mathbf{p}_i^{f,h}\}_{i=1}^{N_v^{f,h}}$ and $\{\mathbf{p}_i^{s,h}\}_{i=1}^{N_v^{s,h}}$ the vertices of meshes $\mathfrak{T}_h^f \cup \mathfrak{T}_h^s$, $\mathfrak{T}_h^f$ and $\mathfrak{T}_h^s$, respectively. Notice that $\mathfrak{T}_h^f$ and $\mathfrak{T}_h^s$ have the same vertices on the interface, then $N_v^h = N_v^{f,h} + N_v^{s,h} - N_v^{I,h}$, being $N_v^{I,h}$ the number of vertices on the interface Γ^I. Analogously, let us denote by $\widetilde{\mathfrak{T}}_h^{f,l}$ and $\widetilde{\mathfrak{T}}_h^{s,l}$ the moved meshes at time t_l, being $\{\mathbf{X}_{\Delta t,h}^l(\mathbf{p}_i^{f,h})\}_{i=1}^{N_v^{f,h}}$ and $\{\mathbf{X}_{\Delta t,h}^l(\mathbf{p}_i^{s,h})\}_{i=1}^{N_v^{s,h}}$ the vertices of these meshes, respectively.

- **Approximation of the material description of the velocity.** It can be easily obtained by using Taylor expansions (4.6) and (4.7). More precisely, since

$$\mathbf{v}_m^{n+1} = \frac{\mathbf{u}^{n+3/2} - \mathbf{u}^{n+1/2}}{\Delta t} + O(\Delta t^2),$$

we define

$$\mathbf{v}_{m,\Delta t,h}^{n+1} := \frac{\mathbf{u}_{\Delta t,h}^{n+3/2} - \mathbf{u}_{\Delta t,h}^{n+1/2}}{\Delta t} \text{ in } \overline{\Omega},$$

for $0 \leq n \leq N-1$.

- **Motion approximation at times $\{t_{n+1}\}_{n=0}^{N-1}$.** Noting that $\mathbf{u}(\mathbf{p},t) = \mathbf{X}(\mathbf{p},t) - \mathbf{p}$ and using (4.6) and (4.7), we obtain

$$\mathbf{X}^{n+1}(\mathbf{p}) = \mathbf{p} + \frac{\mathbf{u}^{n+3/2}(\mathbf{p}) + \mathbf{u}^{n+1/2}(\mathbf{p})}{2} + O(\Delta t^2).$$

Then we define the approximation

$$\mathbf{X}_{\Delta t,h}^{n+1}(\mathbf{p}) := \mathbf{p} + \frac{\mathbf{u}_{\Delta t,h}^{n+3/2}(\mathbf{p}) + \mathbf{u}_{\Delta t,h}^{n+1/2}(\mathbf{p})}{2},$$

for $\mathbf{p} \in \overline{\Omega}$ and $0 \leq n \leq N-1$.

- **Approximation of the spatial description of the velocity.** In order to obtain an approximate velocity in Eulerian coordinates, it will be considered as a piecewise linear function on the

moved mesh $\widetilde{\mathfrak{T}}_h^{f,n+1}\cup\widetilde{\mathfrak{T}}_h^{s,n+1}$, being $\{\mathbf{X}_{\Delta t,h}^{n+1}(\mathbf{p}_i^h)\}_{i=1}^{N_v^h}$ the vertices of this mesh. The values of $\mathbf{v}_{\Delta t,h}^{n+1}$ at vertices $\{\mathbf{X}_{\Delta t,h}^{n+1}(\mathbf{p}_i^h)\}_{i=1}^{N_v^h}$ can be obtained by using $\mathbf{v}_{m,\Delta t,h}^{n+1}$. Since we have

$$\mathbf{v}^{n+1}(\mathbf{X}_{\Delta t,h}^{n+1}(\mathbf{p}_i^h))\simeq\mathbf{v}^{n+1}(\mathbf{X}^{n+1}(\mathbf{p}_i^h))=\mathbf{v}_m^{n+1}(\mathbf{p}_i^h)\simeq\mathbf{v}_{m,\Delta t,h}^{n+1}(\mathbf{p}_i^h),$$

we take the approximation

$$\mathbf{v}_{\Delta t,h}^{n+1}(\mathbf{X}_{\Delta t,h}^{n+1}(\mathbf{p}_i^h)):=\mathbf{v}_{m,\Delta t,h}^{n+1}(\mathbf{p}_i^h),\tag{5.11}$$

for $0\le n\le N-1$. Notice that $\displaystyle\bigcup_{K\in\widetilde{\mathfrak{T}}_h^{f,n+1}\cup\widetilde{\mathfrak{T}}_h^{s,n+1}}K\sim\overline{\Omega}_{t_{n+1}}$.

- **Approximate pressure in spatial coordinates.** In order to approximate this field we use analogous procedures to the ones above. That is, we consider the approximate pressure in spatial coordinates as a piecewise linear function on the moved mesh $\widetilde{\mathfrak{T}}_h^{f,n+1/2}$. The values of the approximate pressure at vertices $\{\mathbf{X}_{\Delta t,h}^{n+1/2}(\mathbf{p}_i^{f,h})\}_{i=1}^{N_v^{f,h}}$ are obtained as follows: firstly, we notice that

$$\pi^{n+1/2}(\mathbf{X}_{\Delta t,h}^{n+1/2}(\mathbf{p}_i^{f,h}))\simeq\pi^{n+1/2}(\mathbf{X}^{n+1/2}(\mathbf{p}_i^{f,h}))=\pi_m^{n+1/2}(\mathbf{p}_i^{f,h})\simeq\pi_{m,\Delta t,h}^{n+1/2}(\mathbf{p}_i^{f,h}),$$

and then we take

$$\pi_{\Delta t,h}^{n+1/2}(\mathbf{X}_{\Delta t,h}^{n+1/2}(\mathbf{p}_i^{f,h})):=\pi_{m,\Delta t,h}^{n+1/2}(\mathbf{p}_i^{f,h}),$$

for $0\le n\le N-1$. Notice that $\displaystyle\bigcup_{K\in\widetilde{\mathfrak{T}}_h^{f,n+1/2}}K\sim\overline{\Omega}_{t_{n+1/2}}^f$.

- **Approximation of the stress tensor in the solid current configuration.** We consider the approximate stress tensor in spatial coordinates as a piecewise linear function on the moved mesh $\widetilde{\mathfrak{T}}_h^{s,n+1/2}$, being $\{\mathbf{X}_{\Delta t,h}^{n+1/2}(\mathbf{p}_i^{s,h})\}_{i=1}^{N_v^{s,h}}$ the vertices of this mesh. The values of the approximate stress tensor at vertices $\{\mathbf{X}_{\Delta t,h}^{n+1/2}(\mathbf{p}_i^{s,h})\}_{i=1}^{N_v^{s,h}}$ are obtained as follows. Firstly, for a given element K^s of the mesh $\mathfrak{T}_h^s$ and a vertex $\mathbf{p}_i^{s,h}\in K^s$, from (3.10) we have

$$\begin{aligned}\mathbf{T}^{n+1/2}(\mathbf{X}_{\Delta t,h}^{n+1/2}(\mathbf{p}_i^{s,h}))&\simeq\mathbf{T}^{n+1/2}(\mathbf{X}^{n+1/2}(\mathbf{p}_i^{s,h}))=\mathbf{T}_m^{n+1/2}(\mathbf{p}_i^{s,h})\\&=\frac{1}{\det\mathbf{F}^{n+1/2}(\mathbf{p}_i^{s,h})}\Big(\lambda\,\mathrm{Div}\,\mathbf{u}(\mathbf{p}_i^{s,h},t_{n+1/2})\mathbf{I}+2\mu\mathcal{E}(\mathbf{u})(\mathbf{p}_i^{s,h},t_{n+1/2})\Big)(\mathbf{F}^{n+1/2})^t(\mathbf{p}_i^{s,h})\\&\simeq\frac{1}{\det\mathbf{F}_{\Delta t,h|K^s}^{n+1/2}}\Big(\lambda(\,\mathrm{Div}\,\mathbf{u}_{\Delta t,h}^{n+1/2})_{|K^s}\mathbf{I}+2\mu\mathcal{E}(\mathbf{u}_{\Delta t,h}^{n+1/2})_{|K^s}\Big)(\mathbf{F}_{\Delta t,h|K^s}^{n+1/2})^t.\end{aligned}$$

Then, we define the approximation

$$\begin{aligned}\mathbf{T}_{\Delta t,h}^{n+1/2}(\mathbf{X}_{\Delta t,h}^{n+1/2}(\mathbf{p}_i^{s,h}))&:=\frac{1}{n_i}\sum_{K^s\in E_i^s}\frac{1}{\det\mathbf{F}_{\Delta t,h|K^s}^{n+1/2}}\Big(\lambda(\,\mathrm{Div}\,\mathbf{u}_{\Delta t,h}^{n+1/2})_{|K^s}\mathbf{I}\\&\quad+2\mu\mathcal{E}(\mathbf{u}_{\Delta t,h}^{n+1/2})_{|K^s}\Big)(\mathbf{F}_{\Delta t,h|K^s}^{n+1/2})^t,\end{aligned}\tag{5.12}$$

for $0\le n\le N-1$, where E_i^s is the set of elements of $\mathfrak{T}_h^s$ that share vertex $\mathbf{p}_i^{s,h}$ and n_i is the number of elements of E_i^s. Notice that $\displaystyle\bigcup_{K\in\widetilde{\mathfrak{T}}_h^{s,n+1/2}}K\sim\overline{\Omega}_{t_{n+1/2}}^s$.

6. Reinitialization of the pure Lagrange-Galerkin scheme. Notice that for pure-Lagrangian schemes, the computational domain is the same for all time steps. However, in order to calculate the velocity, the pressure or the stress tensor in Eulerian coordinates the moved mesh has to be used. For real fluid-structure problems, the fluid mesh may have large deformations. When this happens it is necessary to remesh and reinitialize the motion.

In this section we propose a method to do this for the pure Lagrange-Galerkin scheme (5.4)-(5.10) that preserves the order of convergence. Let us assume that we have decided to reinitialize this problem at time $t_{r-1/2}$ being $1\le r\le N-1$. Then, we first compute $\mathbf{u}_{\Delta t,h}^{r+1/2}$ by using (5.4), (5.5) and (5.8) for $n=r-1$. The objective of this section is the numerical solution of problem (2.5)-(2.8), (3.8)-(3.10) at times $t>t_{r+1/2}$. For this purpose, we first obtain a strong formulation of the problem written in the new reference domain $\overline{\Omega}_{t_{r-1/2}}$ and then we propose a fully discrete scheme by using again a pure-Lagrangian method for time discretization and a finite element approximation for space discretization.

6.1. Strong problem and weak formulation in $\overline{\Omega}_{t_{r-1/2}} \times (t_{r-1/2}, t_f)$. It can be obtained by analogous procedures to the ones in Section 3 but using the change of variable $\mathbf{x} = \mathbf{X}_{t_{r-1/2}}(\mathbf{y}, t)$. Specifically, in order to write equations (2.5), (2.6), (2.7), (3.8) and (3.9) in configuration $\overline{\Omega}_{t_{r-1/2}}$ we use the divergence theorem, the change of variable $\mathbf{x} = \mathbf{X}_{t_{r-1/2}}(\mathbf{y}, t)$, the chain rule and the localization theorem, obtaining

$$\rho_{t_{r-1/2}} \frac{\partial^2 \mathbf{u}_{t_{r-1/2}}}{\partial t^2} - \frac{1}{\det \mathbf{F}_{t_{r-1/2}}} \operatorname{div}_{\mathbf{y}} \left(\mathbf{T}_{t_{r-1/2}} \det \mathbf{F}_{t_{r-1/2}} \mathbf{F}^{-t}_{t_{r-1/2}} \right) = \mathbf{b}_{t_{r-1/2}} \text{ in } \Omega_{t_{r-1/2}} \times (t_0, t_f), \quad (6.1)$$

$$\mathbf{T}_{t_{r-1/2}} = -\pi_{t_{r-1/2}} \mathbf{I} + \eta \left(\operatorname{grad}_{\mathbf{y}} \frac{\partial \mathbf{u}_{t_{r-1/2}}}{\partial t} \mathbf{F}^{-1}_{t_{r-1/2}} + \mathbf{F}^{-t}_{t_{r-1/2}} \left(\operatorname{grad}_{\mathbf{y}} \frac{\partial \mathbf{u}_{t_{r-1/2}}}{\partial t} \right)^t \right)$$
$$\text{in } \Omega^f_{t_{r-1/2}} \times (t_0, t_f), \quad (6.2)$$

$$\operatorname{grad}_{\mathbf{y}} \frac{\partial \mathbf{u}_{t_{r-1/2}}}{\partial t} \cdot \mathbf{F}^{-t}_{t_{r-1/2}} = 0 \quad \text{in } \Omega^f_{t_{r-1/2}} \times (t_0, t_f), \quad (6.3)$$

$$\frac{\partial \mathbf{u}_{t_{r-1/2}}}{\partial t} = (\mathbf{v}_D)_{t_{r-1/2}} \text{ on } \Gamma^D_{t_{r-1/2}} \times (t_0, t_f), \quad (6.4)$$

$$\mathbf{T}_{t_{r-1/2}} \mathbf{F}^{-t}_{t_{r-1/2}} \mathbf{m}_{t_{r-1/2}} = |\mathbf{F}^{-t}_{t_{r-1/2}} \mathbf{m}_{t_{r-1/2}}| \mathbf{h}_{t_{r-1/2}} \text{ on } \Gamma^N_{t_{r-1/2}} \times (t_0, t_f), \quad (6.5)$$

where $\mathbf{m}_{t_{r-1/2}}$ is the outward unit normal vector to $\partial\Omega_{t_{r-1/2}}$.

Remark 6.1. Notice that in this paper we consider a fluid-structure interaction problem in which the solid presents small deformations, that is, the displacement gradient $\nabla \mathbf{u}$ in the solid is small. We want to emphasize that the derivation of the linearized constitutive equation (3.10) is based on this assumption. More precisely, this constitutive equation is obtained neglecting the terms of order $o(\nabla \mathbf{u})$ and assuming the residual stress in the reference configuration ($t = t_0$) vanishes (see [14] for details). Similarly, we can deduce the following linear constitutive equation in configuration $\Omega^s_{t_{r-1/2}}$:

$$\mathbf{T}_{t_{r-1/2}}(\mathbf{y}, t) \det \mathbf{F}_{t_{r-1/2}}(\mathbf{y}, t) \mathbf{F}^{-t}_{t_{r-1/2}}(\mathbf{y}, t) = \lambda \operatorname{div}_{\mathbf{y}} \mathbf{u}_{t_{r-1/2}}(\mathbf{y}, t) \mathbf{I}$$
$$+\mu \left(\operatorname{grad}_{\mathbf{y}} \mathbf{u}_{t_{r-1/2}}(\mathbf{y}, t) + (\operatorname{grad}_{\mathbf{y}} \mathbf{u}_{t_{r-1/2}})^t(\mathbf{y}, t) \right) + \mathbf{T}(\mathbf{y}, t_{r-1/2}), \quad (6.6)$$

for $(\mathbf{y}, t) \in \Omega^s_{t_{r-1/2}} \times (t_0, t_f)$. We notice that $\mathbf{T}(\mathbf{y}, t_{r-1/2})$ is the residual stress tensor at time $t_{r-1/2}$.

Then, in order to obtain an approximate solution of problem (2.5)-(2.8), (3.8)-(3.10) at times $t > t_{r-1/2}$, we need to solve the above boundary value problem for which the following weak formulation can be easily obtained:

$$\int_{\Omega_{t_{r-1/2}}} \rho_{t_{r-1/2}} \det \mathbf{F}_{t_{r-1/2}} \frac{\partial^2 \mathbf{u}_{t_{r-1/2}}}{\partial t^2} \cdot \mathbf{z} \, d\mathbf{y} - \int_{\Omega^f_{t_{r-1/2}}} \pi_{t_{r-1/2}} \det \mathbf{F}_{t_{r-1/2}} \mathbf{F}^{-t}_{t_{r-1/2}} \cdot \operatorname{grad} \mathbf{z} \, d\mathbf{y}$$
$$+\eta \int_{\Omega^f_{t_{r-1/2}}} \left(\operatorname{grad} \frac{\partial \mathbf{u}_{t_{r-1/2}}}{\partial t} \mathbf{F}^{-1}_{t_{r-1/2}} + \mathbf{F}^{-t}_{t_{r-1/2}} \left(\operatorname{grad} \frac{\partial \mathbf{u}_{t_{r-1/2}}}{\partial t} \right)^t \right) \det \mathbf{F}_{t_{r-1/2}} \mathbf{F}^{-t}_{t_{r-1/2}} \cdot \operatorname{grad} \mathbf{z} \, d\mathbf{y}$$
$$+\lambda \int_{\Omega^s_{t_{r-1/2}}} \operatorname{div} \mathbf{u}_{t_{r-1/2}} \operatorname{div} \mathbf{z} \, d\mathbf{y} + 2\mu \int_{\Omega^s_{t_{r-1/2}}} \mathcal{E}(\mathbf{u}_{t_{r-1/2}}) \cdot \mathcal{E}(\mathbf{z}) \, d\mathbf{y}$$
$$= \int_{\Omega_{t_{r-1/2}}} \mathbf{b}_{t_{r-1/2}} \cdot \mathbf{z} \det \mathbf{F}_{t_{r-1/2}} \, d\mathbf{y} - \int_{\Omega^s_{t_{r-1/2}}} \mathbf{T}^{r-1/2} \cdot \operatorname{grad} \mathbf{z} \, d\mathbf{y}$$
$$+ \int_{\Gamma^N_{t_{r-1/2}}} |\mathbf{F}^{-t}_{t_{r-1/2}} \mathbf{m}_{t_{r-1/2}}| \det \mathbf{F}_{t_{r-1/2}} \mathbf{h}_{t_{r-1/2}} \cdot \mathbf{z} \, dA_{\mathbf{y}}, \quad (6.7)$$

$$\int_{\Omega^f_{t_{r-1/2}}} \det \mathbf{F}_{t_{r-1/2}} \operatorname{grad} \frac{\partial \mathbf{u}_{t_{r-1/2}}}{\partial t} \cdot \mathbf{F}^{-t}_{t_{r-1/2}}(\mathbf{y}, t) q \, d\mathbf{y} = 0, \quad (6.8)$$

$\forall \mathbf{z} \in \mathbf{H}^1_{\Gamma^D_{t_{r-1/2}}}(\Omega_{t_{r-1/2}})$, $\forall q \in L^2(\Omega^f_{t_{r-1/2}})$ and where $\mathcal{E}(\Psi) = 1/2(\operatorname{grad} \Psi + (\operatorname{grad} \Psi)^t)$ for a function Ψ.

6.2. Pure Lagrange-Galerkin scheme in $\overline{\Omega}_{t_{r-1/2}} \times (t_{r-1/2}, t_f)$. In what follows we will denote by $\Psi^l_{r-1/2,\Delta t,h}$ approximations of $\Psi^l_{t_{r-1/2}}$ obtained with a fully discretized scheme, being $\Psi = \mathbf{u}$, $\mathbf{X}$, $\mathbf{F}$, π.

An analogous scheme to the one introduced in Section 4 is considered for time discretization of (6.7)-(6.8). More precisely, we take $t = t_{n+1/2}$ in (6.7) and (6.8) and use the second-order formulas (4.1), (4.2)

and (4.3) for $\Psi = \mathbf{u}_{t_{r-1/2}}$. For space discretization, we use continuous piecewise-linear+bubble finite element for each fluid displacement component and continuous piecewise-linear for pressure and each solid displacement component.

Let us suppose $\Omega^f_{t_{r-1/2}}$ and $\Omega^s_{t_{r-1/2}}$ are bounded domains in $\mathbb{R}^d$ with Lipschitz polygonal boundaries. Let us consider suitable families of regular triangulations of $\overline{\Omega}^f_{t_{r-1/2}}$ and $\overline{\Omega}^s_{t_{r-1/2}}$ to be denoted by $\mathfrak{T}_h^{f,r-1/2}$ and $\mathfrak{T}_h^{s,r-1/2}$ respectively, both consisting of elements K of diameter $\leq h$. Moreover, let us assume they have the same vertices on the interface and that they are compatible with the partition of the boundary of $\Omega_{t_{r-1/2}}$ into $\Gamma^D_{t_{r-1/2}}$ and $\Gamma^N_{t_{r-1/2}}$. We consider the following finite element spaces:

$$\mathbf{X}_h^{r-1/2} = \Big\{\mathbf{w}_h \in \big(C^0(\overline{\Omega}_{t_{r-1/2}})\big)^d :\ \mathbf{w}_{h|_K} \in (P_b(K))^d\ \ \forall K \in \mathfrak{T}_h^{f,r-1/2},$$
$$\mathbf{w}_{h|_K} \in (P_1(K))^d\ \ \forall K \in \mathfrak{T}_h^{s,r-1/2}\Big\}, \tag{6.9}$$

$$\mathbf{X}_{0h}^{r-1/2} = \Big\{\mathbf{w}_h \in \mathbf{X}_h^{r-1/2} :\ \mathbf{w}_h = \mathbf{0} \text{ on } \Gamma^D_{t_{r-1/2}}\Big\}, \tag{6.10}$$

$$V_h^{r-1/2} = \Big\{\varphi_h \in C^0(\overline{\Omega}^f_{t_{r-1/2}}) :\ \varphi_{h|_K} \in P_1(K)\ \ \forall K \in \mathfrak{T}_h^{f,r-1/2}\Big\}. \tag{6.11}$$

In order to obtain a fully discrete scheme of the time semidiscretized problem, we replace function spaces $\mathbf{H}^1(\Omega_{t_{r-1/2}})$, $\mathbf{H}^1_{\Gamma^D_{t_{r-1/2}}}(\Omega_{t_{r-1/2}})$ and $L^2(\Omega^f_{t_{r-1/2}})$ with $\mathbf{X}_h^{r-1/2}$, $\mathbf{X}_{0h}^{r-1/2}$ and $V_h^{r-1/2}$, respectively. Now we are in a position to introduce the fully discretized problem:

Pure Lagrange-Galerkin scheme in $\overline{\Omega}_{t_{r-1/2}} \times (t_{r-1/2}, t_f)$. Find two sequences of functions $\widehat{\mathbf{u}}_{r-1/2,\Delta t,h} = \{\mathbf{u}^{n+3/2}_{r-1/2,\Delta t,h}\}_{n=r}^{N-1} \in \Big[\mathbf{X}_h^{r-1/2}\Big]^{N-r}$ and $\widehat{\pi}_{r-1/2,\Delta t,h} = \{\pi^{n+1/2}_{r-1/2,\Delta t,h}\}_{n=r}^{N-1} \in \Big[V_h^{r-1/2}\Big]^{N-r}$ such that

$$\int_{\Omega_{t_{r-1/2}}} \rho^{n+1/2} \circ \mathbf{X}^{n+1/2}_{r-1/2,\Delta t,h} \det \mathbf{F}^{n+1/2}_{r-1/2,\Delta t,h} \frac{\mathbf{u}^{n+3/2}_{r-1/2,\Delta t,h} - 2\mathbf{u}^{n+1/2}_{r-1/2,\Delta t,h} + \mathbf{u}^{n-1/2}_{r-1/2,\Delta t,h}}{\Delta t^2} \cdot \mathbf{z}_h \, d\mathbf{y}$$
$$- \int_{\Omega^f_{t_{r-1/2}}} \pi^{n+1/2}_{r-1/2,\Delta t,h} \det \mathbf{F}^{n+1/2}_{r-1/2,\Delta t,h} (\mathbf{F}^{n+1/2}_{r-1/2,\Delta t,h})^{-t} \cdot \operatorname{grad} \mathbf{z}_h \, d\mathbf{y}$$
$$+\eta \int_{\Omega^f_{t_{r-1/2}}} \det \mathbf{F}^{n+1/2}_{r-1/2,\Delta t,h} \frac{\operatorname{grad} \mathbf{u}^{n+3/2}_{r-1/2,\Delta t,h} - \operatorname{grad} \mathbf{u}^{n-1/2}_{r-1/2,\Delta t,h}}{2\Delta t}$$
$$(\mathbf{F}^{n+1/2}_{r-1/2,\Delta t,h})^{-1} (\mathbf{F}^{n+1/2}_{r-1/2,\Delta t,h})^{-t} \cdot \operatorname{grad} \mathbf{z}_h \, d\mathbf{y} + \eta \int_{\Omega^f_{t_{r-1/2}}} \det \mathbf{F}^{n+1/2}_{r-1/2,\Delta t,h} (\mathbf{F}^{n+1/2}_{r-1/2,\Delta t,h})^{-t}$$
$$\frac{(\operatorname{grad} \mathbf{u}^{n+3/2}_{r-1/2,\Delta t,h})^t - (\operatorname{grad} \mathbf{u}^{n-1/2}_{r-1/2,\Delta t,h})^t}{2\Delta t} (\mathbf{F}^{n+1/2}_{r-1/2,\Delta t,h})^{-t} \cdot \operatorname{grad} \mathbf{z}_h \, d\mathbf{y}$$
$$+\frac{\lambda}{2} \int_{\Omega^s_{t_{r-1/2}}} \Big(\operatorname{div} \mathbf{u}^{n+3/2}_{r-1/2,\Delta t,h} + \operatorname{div} \mathbf{u}^{n-1/2}_{r-1/2,\Delta t,h}\Big) \operatorname{div} \mathbf{z}_h \, d\mathbf{y}$$
$$+\mu \int_{\Omega^s_{t_{r-1/2}}} \Big(\mathcal{E}(\mathbf{u}^{n+3/2}_{r-1/2,\Delta t,h}) + \mathcal{E}(\mathbf{u}^{n-1/2}_{r-1/2,\Delta t,h})\Big) \cdot \mathcal{E}(\mathbf{z}_h) \, d\mathbf{y}$$
$$= \int_{\Omega_{t_{r-1/2}}} \mathbf{b}^{n+1/2} \circ \mathbf{X}^{n+1/2}_{r-1/2,\Delta t,h} \cdot \mathbf{z}_h \det \mathbf{F}^{n+1/2}_{r-1/2,\Delta t,h} \, d\mathbf{y} - \int_{\Omega^s_{t_{r-1/2}}} \mathbf{T}^{r-1/2}_{\Delta t,h} \cdot \operatorname{grad} \mathbf{z}_h \, d\mathbf{y}$$
$$+ \int_{\Gamma^N_{t_{r-1/2}}} |(\mathbf{F}^{n+1/2}_{r-1/2,\Delta t,h})^{-t} \mathbf{m}_{t_{r-1/2}}| \det \mathbf{F}^{n+1/2}_{r-1/2,\Delta t,h} \mathbf{h}^{n+1/2} \circ \mathbf{X}^{n+1/2}_{r-1/2,\Delta t,h} \cdot \mathbf{z}_h \, dA_{\mathbf{y}}, \tag{6.12}$$

$$\int_{\Omega^f_{t_{r-1/2}}} \det \mathbf{F}^{n+1/2}_{r-1/2,\Delta t,h} \frac{\operatorname{grad} \mathbf{u}^{n+3/2}_{r-1/2,\Delta t,h} - \operatorname{grad} \mathbf{u}^{n-1/2}_{r-1/2,\Delta t,h}}{2\Delta t} \cdot (\mathbf{F}^{n+1/2}_{r-1/2,\Delta t,h})^{-t} q_h \, d\mathbf{y} = 0, \tag{6.13}$$

$\forall \mathbf{z}_h \in \mathbf{X}_{0h}^{r-1/2}$, $\forall q_h \in V_h^{r-1/2}$, $r \leq n \leq N-1$, and where

$$\mathbf{X}^{n+1/2}_{r-1/2,\Delta t,h}(\mathbf{y}) := \mathbf{y} + \mathbf{u}^{n+1/2}_{r-1/2,\Delta t,h}(\mathbf{y}),$$
$$\mathbf{F}^{n+1/2}_{r-1/2,\Delta t,h|K} := \mathbf{I} + \operatorname{grad} \mathbf{u}^{n+1/2}_{r-1/2,\Delta t,h|K},$$

for $\mathbf{y} \in \overline{\Omega}_{t_{r-1/2}}$, $K \in \mathfrak{T}_h^{f,r-1/2} \cup \mathfrak{T}_h^{s,r-1/2}$ and $r \leq n \leq N-1$. Notice that stress tensor $\mathbf{T}$ appearing in equation (6.7) is unknown. It is approximated by using (5.12).

Remark 6.2. By using analogous procedures to the ones in Remarks 4.1 and 4.2, we can obtain approximate initial and Dirichlet boundary conditions for displacement $\mathbf{u}_{t_{r-1/2}}$. More precisely, in order to obtain the initial conditions for scheme (6.12)-(6.13), we observe that $\mathbf{u}_{r-1/2}^{r-1/2}(\mathbf{y}) = \mathbf{0}\ \forall \mathbf{y} \in \overline{\Omega}_{t_{r-1/2}}$. Moreover, by using Taylor expansions and that $\mathbf{u}_{r-1/2}^{r-1/2} \equiv \mathbf{0}$, we deduce

$$\mathbf{u}_{r-1/2}^{r+1/2}(\mathbf{y}) = \Delta t \mathbf{v}^r \left(\mathbf{y} + \mathbf{v}^r(\mathbf{y})\frac{1}{2}\Delta t\right) + O(\Delta t^3).$$

Then we take

$$\mathbf{u}_{r-1/2,\Delta t,h}^{r-1/2}(\mathbf{y}) = \mathbf{0},\ \mathbf{u}_{r-1/2,\Delta t,h}^{r+1/2}(\mathbf{y}) = \Delta t \mathbf{v}_{\Delta t,h}^r \left(\mathbf{y} + \mathbf{v}_{\Delta t,h}^r(\mathbf{y})\frac{1}{2}\Delta t\right), \tag{6.14}$$

for all node $\mathbf{y}$ of mesh $\mathfrak{T}_h^{f,r-1/2} \cup \mathfrak{T}_h^{s,r-1/2}$. Notice that, in order to obtain the above approximate initial condition for $\mathbf{u}_{t_{r-1/2}}(\mathbf{y}, t_{r+1/2})$ we need $\mathbf{v}_{\Delta t,h}^r$ that is calculated by (5.11). Similarly, we can obtain approximate Dirichlet boundary conditions for displacement $\mathbf{u}_{t_{r-1/2}}$. More precisely, since

$$\mathbf{u}_{r-1/2}^{n+3/2}(\mathbf{y}) = \mathbf{u}_{r-1/2}^{n-1/2}(\mathbf{y}) + 2\Delta t \mathbf{v}^{n+1/2}\left(\mathbf{X}_{r-1/2}^{n+1/2}(\mathbf{y})\right) + O(\Delta t^3),$$

we deduce the following Dirichlet boundary condition for $\mathbf{u}_{r-1/2}^{n+3/2}$:

$$\mathbf{u}_{r-1/2,\Delta t,h}^{n+3/2}(\mathbf{y}) = \mathbf{u}_{r-1/2,\Delta t,h}^{n-1/2}(\mathbf{y}) + 2\Delta t \mathbf{v}_D^{n+1/2}\left(\mathbf{X}_{r-1/2,\Delta t,h}^{n+1/2}(\mathbf{y})\right), \tag{6.15}$$

for all node y of mesh $\mathfrak{T}_h^{f,r-1/2} \cup \mathfrak{T}_h^{s,r-1/2}$ on Γ^D.

By analogous procedures to the ones in Section 5, we can also obtain, from the solution of problem (6.12)-(6.15), approximations of the pressure in spatial coordinates, the stress tensor in spatial coordinates, the velocity and the motion at time $t > t_{r-1/2}$.

In general, domains at time $t_{r-1/2}$ are unknown, but they are approximated by using the approximate displacement calculated in (5.9).

Then, assuming that we have decided to reinitialize the problem at time $t_{r-1/2}$, the proposed reinitialization algorithm consists of the following steps.

1. Compute the solution of problem (**LG**) for $n = r-2, r-1$ ($\mathbf{u}_{\Delta t,h}^{r-1/2}$ and $\mathbf{u}_{\Delta t,h}^{r+1/2}$) and obtain $\mathbf{X}_{\Delta t,h}^{r-1/2}$ and $\mathbf{v}_{\Delta t,h}^r$ from (5.9) and (5.11).
2. Obtain approximations of domains $\overline{\Omega}_{t_{r-1/2}}^f$ and $\overline{\Omega}_{t_{r-1/2}}^s$ by using $\mathbf{X}_{\Delta t,h}^{r-1/2}$, namely

$$\overline{\Omega}_{t_{r-1/2}}^f \sim \overline{\widetilde{\Omega}}_{t_{r-1/2}}^f := \bigcup_{K \in \widetilde{\mathfrak{T}}_h^{f,r-1/2}} K, \quad \overline{\Omega}_{t_{r-1/2}}^s \sim \overline{\widetilde{\Omega}}_{t_{r-1/2}}^s := \bigcup_{K \in \widetilde{\mathfrak{T}}_h^{s,r-1/2}} K,$$

   being $\{\mathbf{X}_{\Delta t,h}^{r-1/2}(\mathbf{p}_i^{f,h})\}_{i=1}^{N_v^{f,h}}$ (respectively, $\{\mathbf{X}_{\Delta t,h}^{r-1/2}(\mathbf{p}_i^{s,h})\}_{i=1}^{N_v^{s,h}}$) the vertices of mesh $\widetilde{\mathfrak{T}}_h^{f,r-1/2}$ (respectively, $\widetilde{\mathfrak{T}}_h^{s,r-1/2}$).
3. Generate new meshes of domains $\overline{\widetilde{\Omega}}_{t_{r-1/2}}^f$ and $\overline{\widetilde{\Omega}}_{t_{r-1/2}}^s$ which are denoted by $\mathfrak{T}_h^{f,r-1/2}$ and $\mathfrak{T}_h^{s,r-1/2}$ respectively. Notice that $\widetilde{\mathfrak{T}}_h^{f,r-1/2}$ and $\widetilde{\mathfrak{T}}_h^{s,r-1/2}$ are conformal meshes of these domains, but new conformal meshes must be considered in order to not to have meshes with highly distorted elements. In this paper we consider a problem in which the solid presents small deformations but the fluid mesh may have large deformations.
4. Obtain the initial conditions for scheme (6.12)-(6.13) from (6.14), by using $\mathbf{v}_{\Delta t,h}^r$.
5. Solve the linear problem (6.12)-(6.15) where the stress tensor $\mathbf{T}$ appearing in equation (6.7) is approximated by using (5.12).
6. By analogous procedures to the ones in Section 5, we obtain approximations of the pressure in spatial coordinates, the stress tensor in spatial coordinates, the velocity and the motion at time instants $t > t_{r-1/2}$ by using the solution of problem (6.12)-(6.15).

Remark 6.3. This new strategy of reinitialization avoids some difficulties presented by literature methods. For example, in our approach the new domain is updated in a natural way, by using the approximate displacement. Notice that in literature, this domain is obtained by integrating the motion equation ($\dot{\mathbf{X}} = \mathbf{v}_m$) and using an approximate velocity. Moreover, in most reinitialization algorithms of literature, the schemes to solve are non-linear because they are written in the current domain which is unknown. However, we obtain a linear scheme because the problem is written in a previous domain. Moreover, our reinitialization method preserves the order of convergence (second order). For this, it is necessary to start with a high order approximation of displacement $\mathbf{u}_{t_{r-1/2}}$ as (6.14).

7. Numerical results. In order to assess the performance of the numerical method introduced in this article, we solve three test problems in two space dimensions. The first one is an academic problem which is used to check the convergence rates. The second one is the 2D motion of an elastic circular cylinder in a tank filled with an incompressible Newtonian viscous fluid. Different values for the density of the cylinder and the fluid viscosity are considered. This problem has been solved with the method described in the present paper, being necessary to remesh and to reinitialize the motion from time to time. Finally, the third example is a free surface problem. More precisely, we consider an example of 2D sloshing of an incompressible Newtonian viscous fluid where a circular cylinder is submerged.

In Example 1, we calculate the error between discrete solutions $\mathbf{u}_{\Delta t,h}$, $\mathbf{v}_{\Delta t,h}$, $\pi_{\Delta t,h}$, and exact solutions $\mathbf{u}$, $\mathbf{v}$, π. For this, we approximate the theoretical $H^1(\Omega_\tau)$ and $L^2(\Omega_\tau)$ norms by using a quadrature formula exact for polynomials of degree 5. Moreover, domain at time τ with $\tau > t_0$, is calculated by using the approximate motion. The function spaces endowed with these norms are denoted by $H^1_h(\Omega_\tau)$ and $L^2_h(\Omega_\tau)$, respectively. Furthermore, we introduce the notation $\mathbf{H}^1_h(\Omega_\tau) = (H^1_h(\Omega_\tau))^2$, $\mathbf{L}^2_h(\Omega_\tau) = (L^2_h(\Omega_\tau))^2$ and denote by $l^\infty(\mathcal{A}^n)$ the space of sequences in $\mathcal{A}^n$ equipped with the norm $\left|\left|\widehat{\Psi}\right|\right|_{l^\infty(\mathcal{A}^n)} := \max_n ||\Psi^n||_{\mathcal{A}^n}$, being $\mathcal{A}^n$ one of the following spaces:

$$\mathbf{L}^2_h(\Omega), \mathbf{H}^1_h(\Omega), \mathbf{L}^2_h(\Omega_{t_{n+1}}), \mathbf{H}^1_h(\Omega_{t_{n+1}}), L^2_h(\Omega_{t_{n+1/2}}), H^1_h(\Omega_{t_{n+1/2}}).$$

Moreover, all integrals appearing in the discrete weak formulations introduced above are approximated by using an exact quadrature formula for polynomials of degree 5.

Example 1

This is a problem aiming to analyze the rates of convergence. The fluid domain is $\Omega^f = (0,1) \times (0,1)$ and the solid domain is $\Omega^s = (1,2) \times (0,1)$, the initial time is $t_0 = 0$ and the final time is $t_f = 1$. The physical parameters are $\rho = 1$, $\lambda = 1$, $\mu = 1$ and $\eta = 0.1$. We adjust the body force and the boundary conditions so that the solution of the problem is the following:

$$\begin{aligned}\mathbf{v}(x_1, x_2, t) &= (0.01\exp(t), 0.01\exp(t)\cos(x_1 - 0.01\exp(t) - 1)),\\ \pi(x_1, x_2, t) &= \exp(t)\sin(x_1 - 0.01\exp(t) - 1),\\ \mathbf{u}(p_1, p_2, t) &= (0.01\exp(t), 0.01\exp(t)\cos(p_1 - 1)).\end{aligned}$$

Notice that for this example, equations (3.21) and (3.22) are satisfied. We have solved this problem

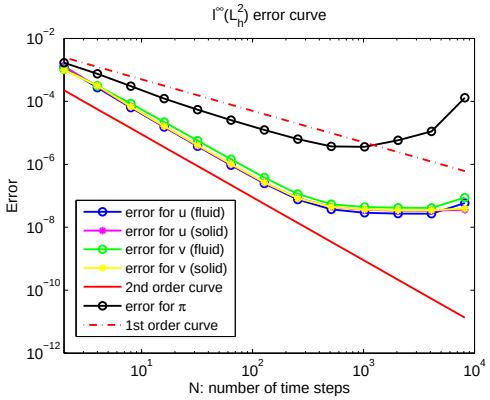

FIG. 7.1. *Example 1: computed $l^\infty(L^2_h)$ errors, in log-log scale, versus the number of time steps for a fixed spatial mesh of* 251×251 *vertices.*

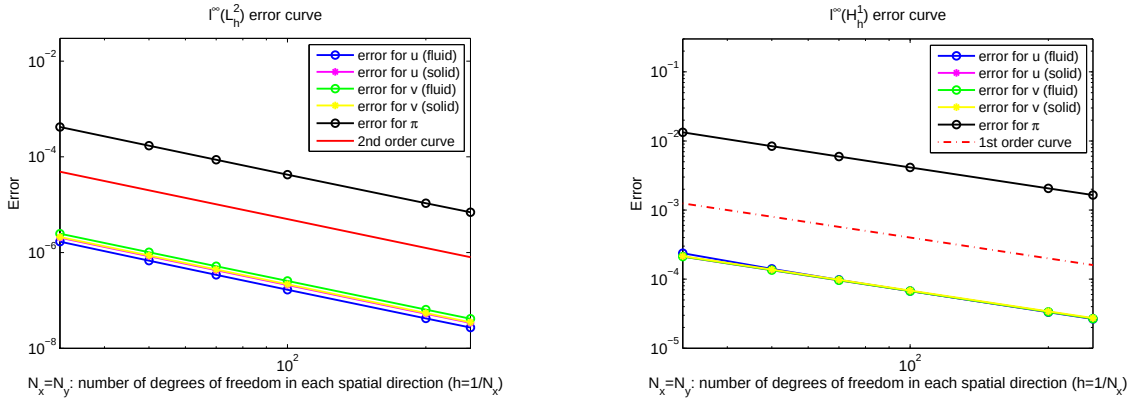

FIG. 7.2. *Example 1: computed* $l^\infty(L_h^2)$ *(left) and* $l^\infty(H_h^1)$ *(right) errors, in log-log scale, versus* $1/h$ *for* $\Delta t = 1/2500$.

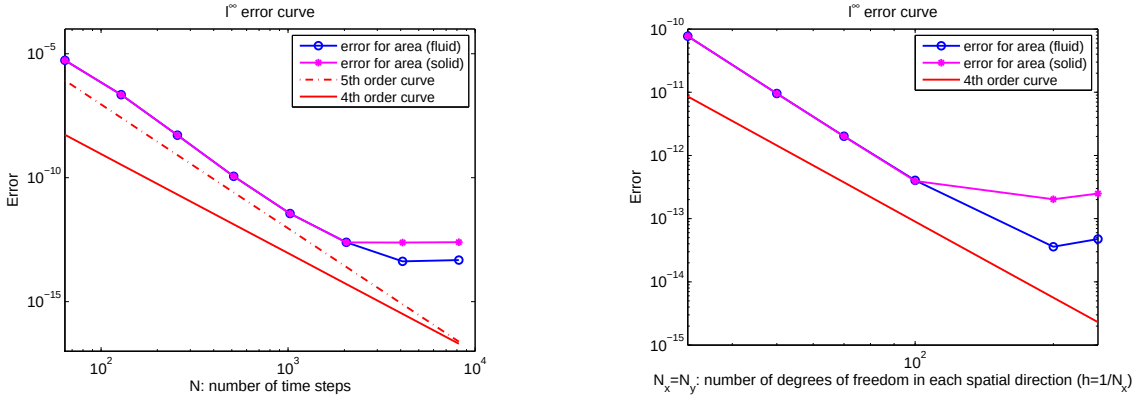

FIG. 7.3. *Example 1: on the left, computed* l^∞ *errors for areas, in log-log scale, versus the number of time steps for a fixed spatial mesh of* 251×251 *vertices and for* $t_f = 4$. *On the right, computed* l^∞ *errors for areas, in log-log scale, versus* $1/h$ *for* $\Delta t = 1/2048$ *and for* $t_f = 4$.

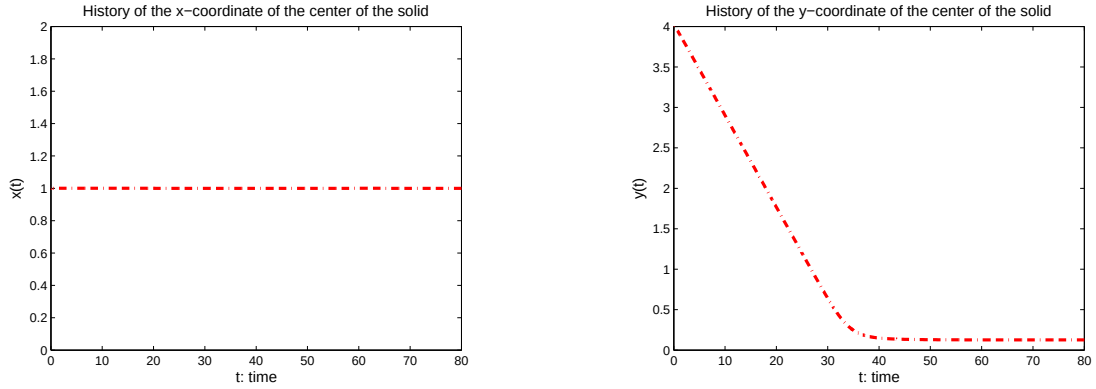

FIG. 7.4. *2D Motion of a cylinder: histories of the x-coordinate (left) and y-coordinate (right) of the solid center for* $\eta = 0.1$ *and* $\rho^s = 1.25$, *and for* $\Delta t = 0.02$.

by using the Lagrange-Galerkin method introduced in this paper (**LG**) with and without reinitializing. However, we only present the results obtained without any reinitialization, because the errors observed for velocity and pressure are practically the same in both cases. The initial conditions $\mathbf{u}_{\Delta t,h}^{-1/2}$ and $\mathbf{u}_{\Delta t,h}^{1/2}$ are calculated by (5.6) and (5.7), respectively. In Figure 7.1, we have fixed a uniform spatial mesh of 251×251 vertices and show the $l^\infty\left(\mathbf{L}_h^2(\Omega)\right)$ displacement error, the $l^\infty\left(\mathbf{L}_h^2(\Omega_{t_{n+1}})\right)$ velocity error and the $l^\infty\left(L_h^2(\Omega_{t_{n+1/2}})\right)$ pressure error versus the number of time steps. These results show that the scheme (**LG**) possesses second-order accuracy in time for displacement and velocity and first-order accuracy in time for pressure. Notice that, for fixed h, we can observe an increasing error as the time step decreases below a threshold. This seems to be due to the fact that terms with Δt in the denominator would be

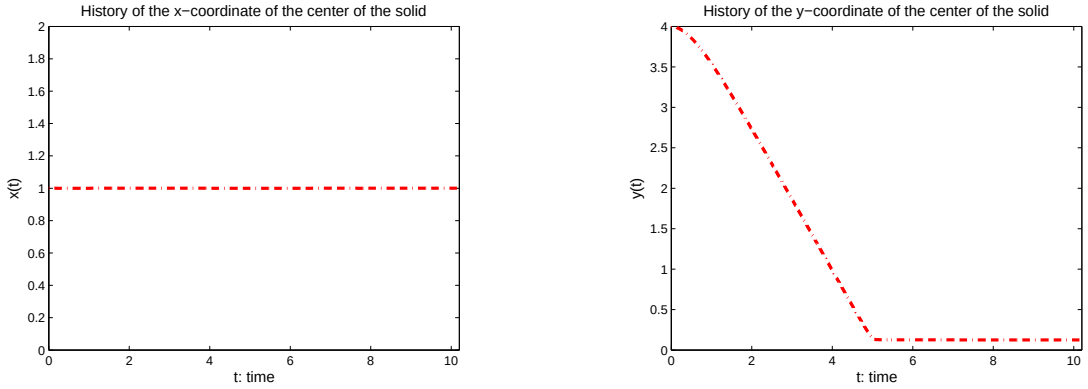

FIG. 7.5. *2D Motion of a cylinder: histories of the x-coordinate (left) and y-coordinate (right) of the solid center for* $\eta = 0.01$ *and* $\rho^s = 1.5$*, and for* $\Delta t = 0.001$.

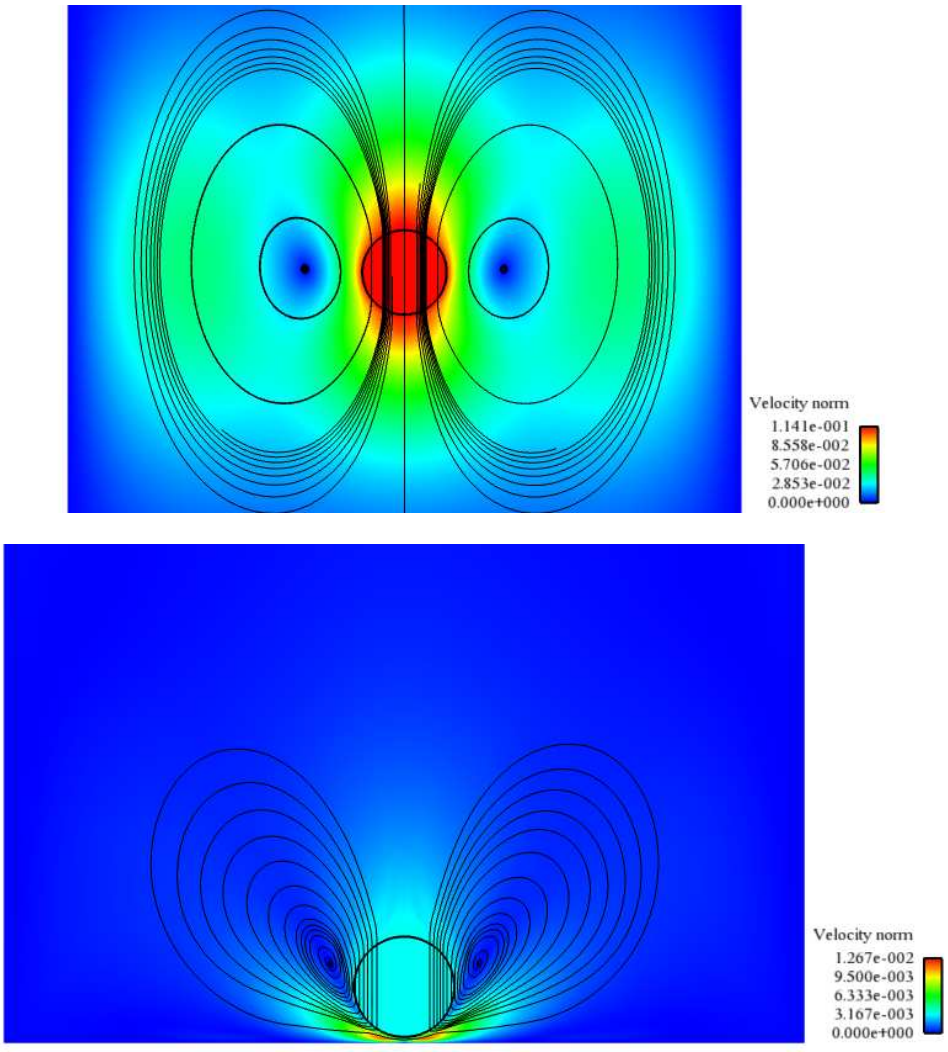

FIG. 7.6. *2D Motion of a cylinder: numerical streamlines for* $\eta = 0.1$ *and* $\rho^s = 1.25$ *at* $t = 14.3$ *and* $t = 42$*, respectively, and for* $\Delta t = 0.02$.

present in the error expression due to the need of using quadrature formulas. It is well-known (see, for instance, [23], [21], [29], [24], [30], [8], [3]) that the numerical integration in Lagrange-Galerkin methods may add terms to the final error of the form $O(h^\alpha/\Delta t)$ and, in some cases, even it produces the loss of unconditional stability. In Figure 7.2 we represent the computed $l^\infty\left(L_h^2\right)$ and $l^\infty\left(H_h^1\right)$ errors for displacement, velocity and pressure versus $1/h$, for a fixed small time step, namely $\Delta t = 0.0004$. We

can observe that the (**LG**) scheme possesses second-order accuracy in space in the $l^\infty(L^2_h)$-norm and first-order accuracy in space in the $l^\infty(H^1_h)$-norm.

Moreover, for this example we have also numerically checked that the scheme conserves the volume with high order of accuracy. Notice that in this example $\det \mathbf{F} = 1$ in the fluid domain and in the solid domain, therefore the areas occupied by fluid and solid are conserved along the time ($area(\Omega^f_t) = area(\Omega^f)$, $area(\Omega^s_t) = area(\Omega^s)$ $\forall t$). Then we calculate the l^∞ errors between the areas of fluid and solid domains at times $\{t_{n+1/2}\}_n$ (calculated by using the approximate motion) and the exact areas ($area(\Omega^s)$ and $area(\Omega^f)$), i.e., we compute the errors

$$\max_n \left| area(\Omega^f_{t_{n+1/2}}) - area(\Omega^f) \right|, \quad \max_n \left| area(\Omega^s_{t_{n+1/2}}) - area(\Omega^s) \right|,$$

where domains $\Omega^f_{t_{n+1/2}}$ and $\Omega^s_{t_{n+1/2}}$ are calculated by using the approximate motion. In Figure 7.3 (on the left) we represent these l^∞ errors versus the number of time steps for a fixed uniform spatial mesh of 251×251 vertices and for $t_f = 4$. In Figure 7.3 (on the right), we have fixed the time step, namely $\Delta t = 1/2048$, and show the l^∞ errors for the areas versus $1/h$ for $t_f = 4$.

FIG. 7.7. *2D Motion of a cylinder: isopressure contours for* $\eta = 0.1$ *and* $\rho^s = 1.25$ *at* $t = 14.295$ *and* $t = 41.99$, *respectively, and for* $\Delta t = 0.02$.

Example 2

In this example we consider the 2D motion of an elastic circular cylinder in a rectangular cavity filled with an incompressible Newtonian viscous fluid. The only force considered is gravity. The computational domain is $\Omega = (0, 2) \times (0, 6)$, the diameter of the cylinder is $d = 0.25$ and the fluid density is $\rho^f = 1$. The values of the Young modulus and Poisson ratio for the cylinder are 10^8 and 0.3, respectively. For these values, the solid is visually non-deformable. We solve this problem for different viscosity coefficients ($\eta = 0.1$, $\eta = 0.01$) and for different solid densities ($\rho^s = 0.5$, $\rho^s = 1.25$, $\rho^s = 1.5$), with the pure-Lagrangian method (**LG**), but remeshing and reinitializing the motion at some times. Specifically, for $\eta = 0.1$ (respectively, for $\eta = 0.01$) the problem is reinitialized every second being $\Delta t = 0.02$ (respectively, every 0.01 seconds being $\Delta t = 0.001$). The fluid and the solid are initially at rest. Moreover, when $\rho^s > \rho^f$ the fluid velocity is $\mathbf{0}$ on the boundary of Ω, that is $\mathbf{v}_D \equiv \mathbf{0}$. However, when $\rho^s < \rho^f$, we impose null Neumann condition (force-free) on the upper horizontal boundary, while on the vertical boundaries and on the lower horizontal boundary the velocity is zero (no-slip boundary condition). The considered Lagrangian meshes are finer close to the cylinder. More precisely, for all meshes the minimum mesh-size is $h_{min} = 0.001$ and the maximum one is $h_{max} = 0.07$. In Figures 7.4 and 7.5 we show the x-coordinate and y-coordinate of the center of the solid along the time for $\mu = 0.1$, $\rho^s = 1.25$ and for $\mu = 0.01$, $\rho^s = 1.5$, respectively. As expected, we can observe that the cylinder falls much faster when its density is increased and the fluid viscosity is reduced. In Figures 7.6 and 7.7 we represent, respectively, the streamlines and the isopressure contours at two times for $\mu = 0.1$ and $\rho^s = 1.25$. Similarly, in Figures 7.8 and 7.9 the streamlines and the isopressure contours at two times and for $\mu = 0.01$ and $\rho^s = 1.5$ are shown, respectively. As expected, we obtain a recirculating motion and a symmetric solution. In particular, for both

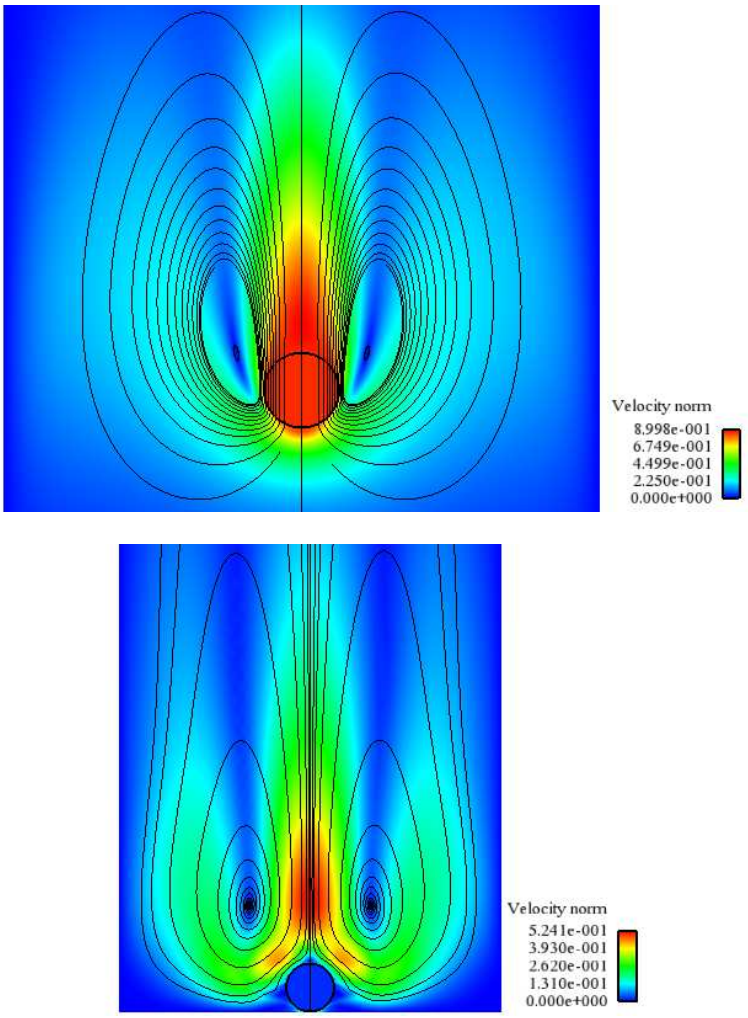

FIG. 7.8. *2D Motion of a cylinder: numerical streamlines for* $\eta = 0.01$ *and* $\rho^s = 1.5$ *at* $t = 2.25$ *and* $t = 5.49$*, respectively, and for* $\Delta t = 0.001$.

FIG. 7.9. *2D Motion of a cylinder: isopressure contours for* $\eta = 0.01$ *and* $\rho^s = 1.5$ *at* $t = 2.2495$ *and* $t = 5.4895$*, respectively, and for* $\Delta t = 0.001$.

experiments, two perfect symmetric eddies are obtained at each time. These features can be observed in figures 7.6-7.9. Notice that these experiments have been solved in the whole domain. It is remarkable that

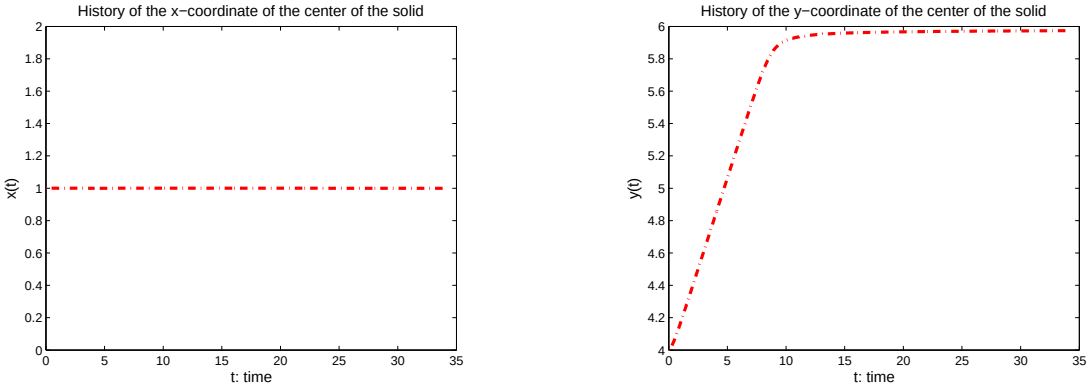

FIG. 7.10. *2D Motion of a cylinder: histories of the x-coordinate (left) and y-coordinate (right) of the solid center for* $\eta = 0.1$ *and* $\rho^s = 0.5$*, and for* $\Delta t = 0.02$.

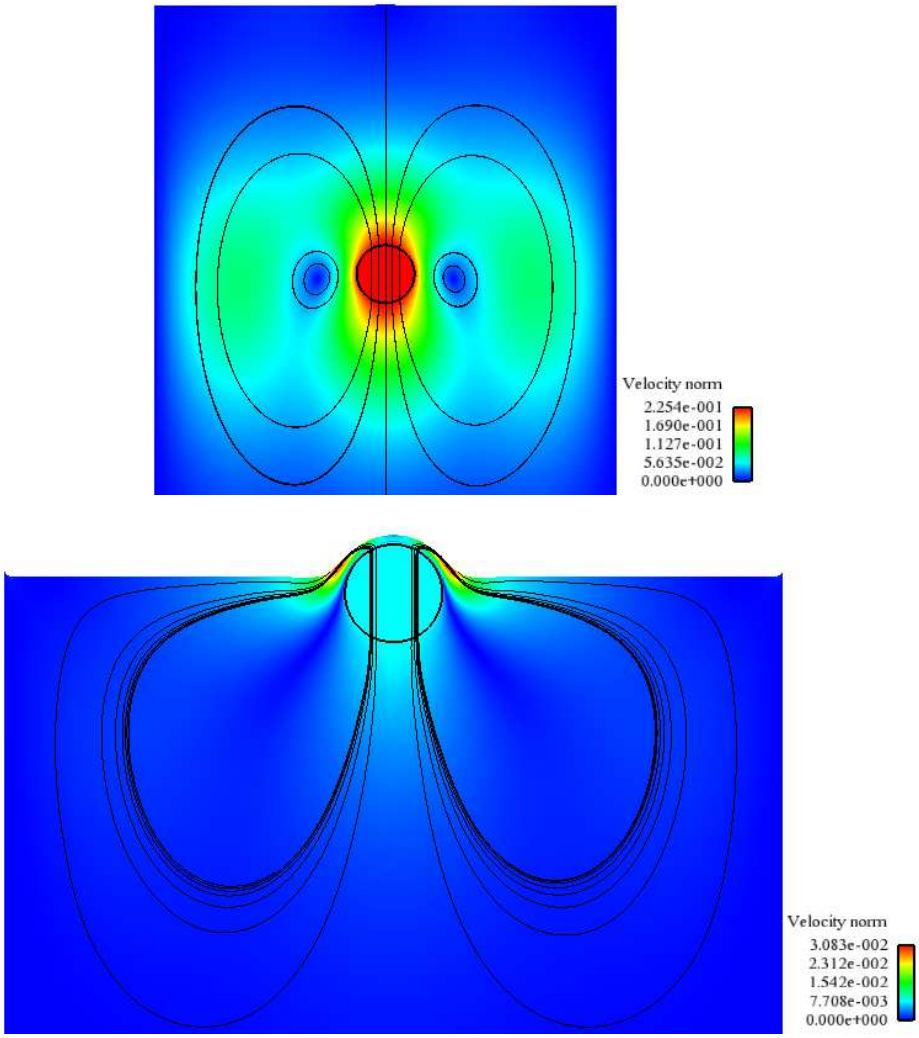

FIG. 7.11. *2D Motion of a cylinder: numerical streamlines for* $\eta = 0.1$ *and* $\rho^s = 0.5$ *at* $t = 4$ *and* $t = 12$*, respectively, and for* $\Delta t = 0.02$.

the scheme is accurate even at very small scales. In particular, in Figures 7.6 and 7.8 we can see the good definition of the streamlines even at very small scales. Moreover, as we can see in Figures 7.7 and 7.9, decreasing Reynolds number, the hydrostatic pressure becomes increasingly prominent. In [13] numerical results for similar experiments are presented. Qualitatively, some of our results are in good agreement with those presented in [13]. Moreover, we show the numerical results obtained for $\mu = 0.1$ and $\rho^s = 0.5$.

FIG. 7.12. *2D Motion of a cylinder: isopressure contours for* $\eta = 0.1$ *and* $\rho^s = 0.5$ *at* $t = 3.99$ *and* $t = 11.99$*, respectively, and for* $\Delta t = 0.02$*.*

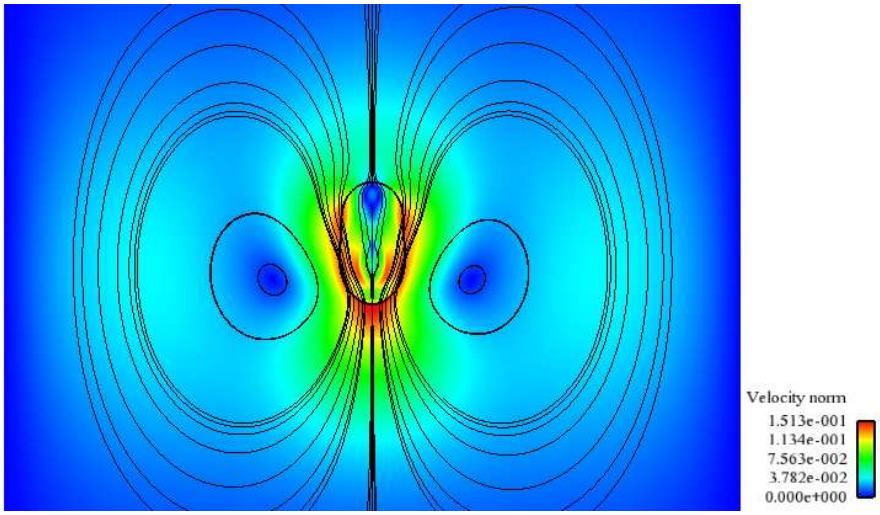

FIG. 7.13. *2D Motion of a cylinder: numerical streamlines for* $\eta = 0.1$*,* $\rho^s = 1.25$*,* $E = 2$ *and* $\nu = 0.3$ *at* $t = 1$*, for* $\Delta t = 0.02$*.*

More precisely, in Figures 7.10, 7.11 and 7.12 we show the x-coordinate and y-coordinate of the center of the solid along the time and the streamlines and the isopressure contours at two times, respectively. Finally, in order to show the behaviour of the pure-Lagrangian scheme for large solid deformation, we solve the problem described above for $\eta = 0.1$, $\rho^s = 1.25$, $E = 2$ and $\nu = 0.3$, with the pure-Lagrangian method (**LG**). The obtained results are depicted in Figures 7.13 and 7.14 where the streamlines at $t = 1$ and the isopressure contours at $t = 0.99$ are shown, respectively. In this case any reinitialization was not done.

Example 3

In this example we simulate the large amplitude 2D sloshing of a fluid with a submerged cylinder. There are several papers in the literature solving this problem but without the submerged body (see, for instance, [16], [28] and [2]). The width of the tank is $0.8\,m$, its depth is $0.3\,m$ and the diameter of the cylinder is $d = 0.12\,m$. The values of the Young modulus and Poisson ratio for the solid are 10^8 and 0.3, respectively. The liquid in the tank is subject to a sinusoidal horizontal force. More precisely, the body force is

$$\mathbf{b}(\mathbf{x}, t) = \rho(\mathbf{x}, t)(Ag\sin(\omega t), -g),$$

where A is an arbitrary constant governing the amplitude of the excitation, g is the gravity acceleration and ω is the excitation frequency. We have taken, $A = 0.01$, $\rho = 1000\,kg/m^3$, $g = 9.8\,m/s^2$ and

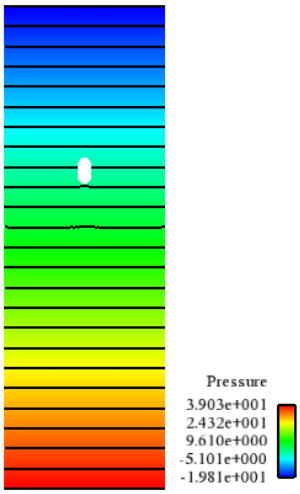

FIG. 7.14. *2D Motion of a cylinder: isopressure contours for* $\eta = 0.1$, $\rho^s = 1.25$, $E = 2$ *and* $\nu = 0.3$ *at* $t = 0.99$, *for* $\Delta t = 0.02$.

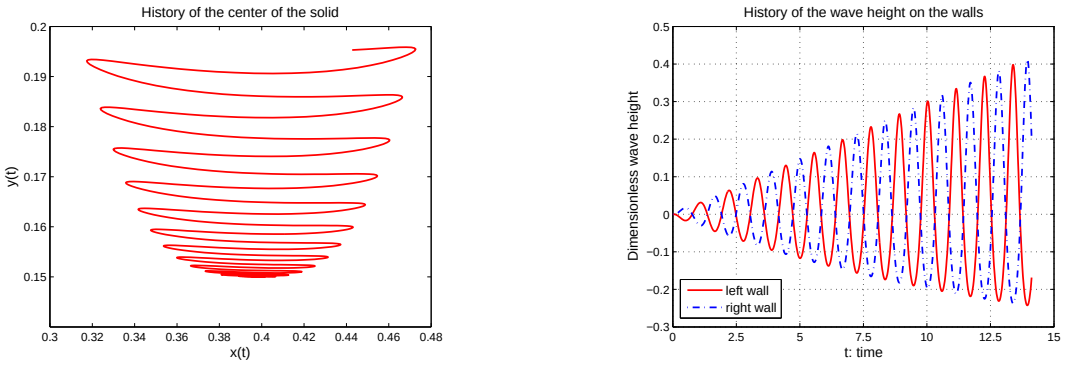

FIG. 7.15. *Sloshing waves: histories of the center of the solid (left) and of wave height at the walls (right), for a spatial mesh of* 11097 *vertices and* $\Delta t = 0.02$.

$\omega = 5.642\, rad/s$. Using these parameters, experimental results show that the first resonance frequency of the tank filled with inviscid fluid and using the potential theory is $0.898 Hz$. Moreover, the viscosity coefficient has been taken $\eta = 1 Pa.s$. The only body force acting on the solid is gravity. On the vertical boundaries the horizontal velocity is zero, on the lower horizontal boundary the vertical velocity is zero and on the upper horizontal boundary we impose null Neumann condition (force-free). In order to show the behaviour of the pure-Lagrangian scheme for large mesh distortion, we solve this problem with the pure-Lagrangian method (**LG**) without any reinitialization. In this method, at each time step, the computational domain is the reference domain; in this case it is $\Omega = (0, 0.8) \times (0, 0.3)$. The computational time of this simulation, with the pure-Lagrangian method (**LG**) without any reinitialization (on a DELL PowerEdge computer with an Intel(R) Xeon(R) processor, CPU E5430 @ 2.66GHz, and 16GB of RAM) and for a spatial mesh of 11097 vertices, $\Delta t = 0.02$ and $t_f = 14.13$, is 3.85 min. In particular, the computational time per time step spent in solving the Navier-Stokes equations is 0.33 s. Notice that, at each time step we solve a linear problem. However, most schemes in literature solve non-linear problems.

Figure (7.15) shows the trajectory of the center of the solid (left) and the vertical displacement of the upper corner nodes at the tank wall as a function of time (right). In Figure 7.16 we represent an instantaneous configuration of the domain, the streamlines and the isopressure contours.

Moreover, for this example we have also numerically checked that the scheme conserves the fluid volume: the relative error at the final time ($t_f = 14.13$) and the l^∞ relative error, in the fluid area, are $2.738E-04$ and $3.613E-04$, respectively, for a spatial mesh of 11097 vertices and $\Delta t = 0.02$.

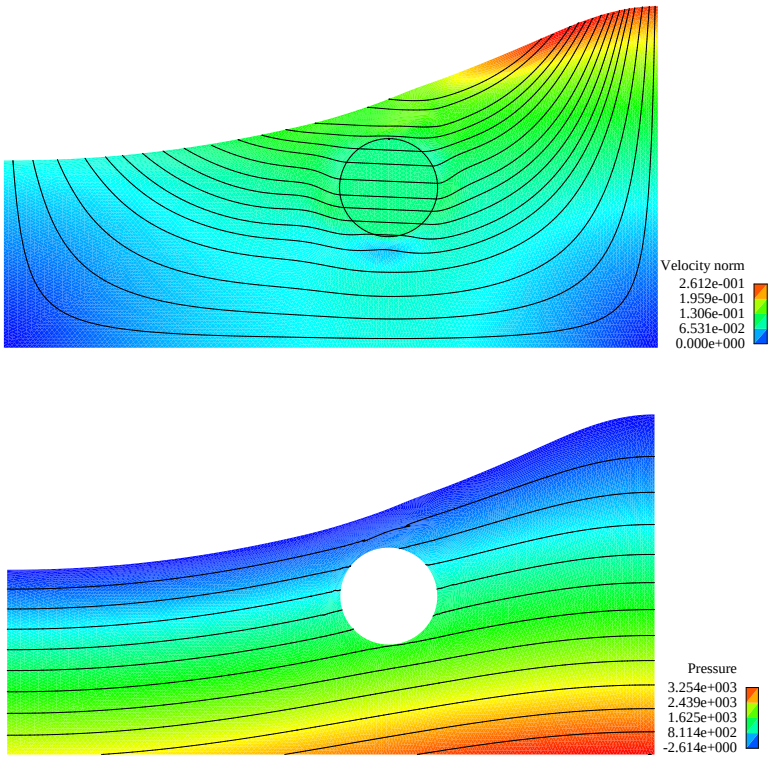

FIG. 7.16. *Sloshing waves: instantaneous domain configuration, streamlines and isopressure contours at* $t = 14$ *and* $t = 13.99$*, respectively, and for a spatial mesh of* 11097 *vertices and* $\Delta t = 0.02$.

8. Conclusions. We have introduced a pure Lagrange-Galerkin scheme for solving fluid-structure interaction problems. This scheme is written in Lagrangian coordinates and in terms of displacement rather than velocity also for the fluid and therefore it is useful for solving free surface and fluid-structure interaction problems. For moderate to high-Reynolds number flows, this scheme can lead to high distortion in the mesh elements. When this happens it is necessary to remesh and reinitialize the scheme from time to time. We have proposed a method for reinitialization. Numerical tests have been presented to assess the effectiveness of the method and to analyze its rates of convergence. In particular, we have considered the 2D motion of an elastic cylinder in a rectangular tank filled with an incompressible Newtonian viscous fluid. This problem has been solved with the pure-Lagrangian method but remeshing and reinitializing at certain times were needed. Moreover, we have considered a 2D sloshing problem of a fluid containing an elastic submerged cylinder that has been solved without any reinitialization. We have also numerically checked that the scheme conserves the volume with high order of accuracy both in time and in space.

REFERENCES

[1] D. N. ARNOLD AND M. FORTIN, *A stable finite element for the Stokes equations*, Calcolo, 21 (1984), pp. 337–344.
[2] M. BENÍTEZ AND A. BERMÚDEZ, *Pure lagrangian and semi-lagrangian finite element methods for the numerical solution of Navier-Stokes equations*, Appl. Numer. Math., to appear.
[3] ———, *A second order characteristics finite element scheme for natural convection problems*, J. Comput. Appl. Math., 235 (2011), pp. 3270–3284.
[4] ———, *Numerical Analysis of a second-order pure Lagrange-Galerkin method for convection-diffusion problems. Part I: time discretization*, SIAM. J. Numer. Anal., 50 (2012), pp. 858–882.
[5] ———, *Numerical Analysis of a second-order pure Lagrange-Galerkin method for convection-diffusion problems. Part II: fully discretized scheme and numerical results*, SIAM. J. Numer. Anal., 50 (2012), pp. 2824–2844.
[6] ———, *Pure Lagrangian and semi-Lagrangian finite element methods for the numerical solution of convection-diffusion problems*, Int. J. Numer. Anal. Mod., 11 (2014), pp. 271–287.
[7] A. BERMÚDEZ, M. R. NOGUEIRAS, AND C. VÁZQUEZ, *Numerical analysis of convection-diffusion-reaction problems with higher order characteristics/finite elements. Part I: Time discretization*, SIAM. J. Numer. Anal., 44 (2006), pp. 1829–1853.
[8] ———, *Numerical analysis of convection-diffusion-reaction problems with higher order characteristics/finite elements.*

Part II: Fully discretized scheme and quadrature formulas, SIAM. J. Numer. Anal., 44 (2006), pp. 1854–1876.

[9] K. Chrysafinos and N. J. Walkington, *Lagrangian and moving mesh methods for the convection diffusion equation*, M2AN Math. Model. Numer. Anal., 42 (2008), pp. 25–55.

[10] F. Del Pin, S. Idelsohn, E. Oñate, and R. Aubry, *The ale/lagrangian particle finite element method: A new approach to computation of free-surface flows and fluid-object interactions*, Comput. Fluids, 36 (2007), pp. 27–38.

[11] J. Douglas, Jr., and T. F. Russell, *Numerical methods for convection-dominated diffusion problems based on combining the method of characteristics with finite element or finite difference procedures*, SIAM J. Numer. Anal., 19 (1982), pp. 871–885.

[12] R. E. Ewing and H. Wang, *A summary of numerical methods for time-dependent advection-dominated partial differential equations*, J. Comput. Appl. Math., 128 (2001), pp. 423–445.

[13] R. Glowinski, T. W. Pan, T. I. Hesla, D. D. Joseph, and J. Périauxz, *A fictitious domain approach to the direct numerical simulation of incompressible viscous flow past moving rigid bodies: application to particulate flow*, J. Comput. Phys., 169 (2001), pp. 363–423.

[14] M. E. Gurtin, *An Introduction to Continuum Mechanics*, vol. 158, Academic Press, San Diego, 1981.

[15] C. W. Hirt, J. L. Cook, and T. D. Butler, *A lagrangian method for calculation of the dynamics of an incompressible fluid with a free surface*, J. Comput. Phys., 5 (1970), pp. 103–124.

[16] A. Huerta and W. K. Liu, *Viscous flow with large free surface motion*, Comput. Methods Appl. Mech. Engrg., 69 (1988), pp. 277–324.

[17] S. Idelsohn, J. Marti, A. Limache, and E. Oñate, *Unified lagrangian formulation for elastic solids and incompressible fluids: Application to fluid-structure interaction problems via the pfem*, Comput. Methods in Appl. Mech. Eng., 197 (2008), pp. 1762–1776.

[18] S. Idelsohn, E. Oñate, and F. Del Pin, *The particle finite element method: a powerful tool to solve incompressible flows with free-surfaces and breaking waves*, Int. J. Numer. Meth. Eng., 61 (2004), pp. 964–989.

[19] S. Idelsohn, E. Oñate, F. Del Pin, and N. Calvo, *Fluid-structure interaction using the particle finite element method*, Comput. Methods in Appl. Mech. Eng., 195 (2006), pp. 2100–2123.

[20] M. Kawahara and A. Anjyu, *Lagrangian finite element method for solitary wave propagation*, Comput. Mech., 3 (1988), pp. 299–307.

[21] K. W. Morton, A. Priestley, and E. Süli, *Stability of the Lagrange-Galerkin method with non-exact integration*, M2AN Math. Model. Numer. Anal., 22 (1998), pp. 625–653.

[22] E. Oñate, S. Idelsohn, M. A. Celigueta, and R. Rossi, *Advances in the particle finite element method for the analysis of fluid-multibody interaction and bed erosion in free surface flows*, Comput. Methods in Appl. Mech. Eng., 197 (2008), pp. 1777–1800.

[23] O. Pironneau, *On the transport-diffusion algorithm and its applications to the Navier-Stokes equations*, Numer. Math., 38 (1982), pp. 309–332.

[24] A. Priestley, *Exact projections and the Lagrange-Galerkin method: a realistic alternative to quadrature*, J. Comput. Phys., 112 (1994), pp. 316–333.

[25] R. Radovitzky and M. Ortiz, *Lagrangian finite element analysis of newtonian fluid flows*, Int. J. Numer. Meth. Engng., 43 (1998), pp. 607–619.

[26] B. Ramaswamy and M. Kawahara, *Lagrangian finite element analysis applied to viscous free surface fluid flow*, Int. J. Numer. Meth. Fluids, 7 (1987), pp. 953–984.

[27] H. Rui and M. Tabata, *A second order characteristic finite element scheme for convection-diffusion problems*, Numer. Math., 92 (2002), pp. 161–177.

[28] M. Souli and J. P. Zolesio, *Arbitrary Lagrangian-Eulerian and free surface methods in fluid mechanics*, Comput. Methods Appl. Mech. Engrg., 191 (2001), pp. 451–466.

[29] E. Süli, *Stability and convergence of the Lagrange-Galerkin method with non-exact integration. Academic Press, London*, The mathematics of finite elements and applications, VI, (1988), pp. 435–442.

[30] M. Tabata and S. Fujima, *Robustness of a characteristic finite element scheme of second order in time increment*, Computational Fluid Dynamics 2004, (2006), pp. 177–182.